POLITECNICO DI TORINO
Repository ISTITUZIONALE

Measurement of prompt D0, D+, D*+, and DS+ production in p–Pb collisions at sNN = 5.02 TeV

(Article begins on next page)

02 May 2024

Measurement of prompt D^0, D^+, D^{*+}, and D_s^+ production in p–Pb collisions at $\sqrt{s_{NN}} = 5.02$ TeV

The ALICE collaboration

E-mail: ALICE-publications@cern.ch

ABSTRACT: The measurement of the production of prompt D^0, D^+, D^{*+}, and D_s^+ mesons in proton–lead (p–Pb) collisions at the centre-of-mass energy per nucleon pair of $\sqrt{s_{NN}} = 5.02$ TeV, with an integrated luminosity of $292 \pm 11\,\mu\text{b}^{-1}$, are reported. Differential production cross sections are measured at mid-rapidity ($-0.96 < y_{\text{cms}} < 0.04$) as a function of transverse momentum (p_T) in the intervals $0 < p_T < 36$ GeV/c for D^0, $1 < p_T < 36$ GeV/c for D^+ and D^{*+}, and $2 < p_T < 24$ GeV/c for D_s^+ mesons. For each species, the nuclear modification factor R_{pPb} is calculated as a function of p_T using a proton-proton (pp) reference measured at the same collision energy. The results are compatible with unity in the whole p_T range. The average of the non-strange D mesons R_{pPb} is compared with theoretical model predictions that include initial-state effects and parton transport model predictions. The p_T dependence of the D^0, D^+, and D^{*+} nuclear modification factors is also reported in the interval $1 < p_T < 36$ GeV/c as a function of the collision centrality, and the central-to-peripheral ratios are computed from the D-meson yields measured in different centrality classes. The results are further compared with charged-particle measurements and a similar trend is observed in all the centrality classes. The ratios of the p_T-differential cross sections of D^0, D^+, D^{*+}, and D_s^+ mesons are also reported. The D_s^+ and D^+ yields are compared as a function of the charged-particle multiplicity for several p_T intervals. No modification in the relative abundances of the four species is observed with respect to pp collisions within the statistical and systematic uncertainties.

https://doi.org/10.1007/JHEP12(2019)092

Contents

1 Introduction

Measurements of heavy-flavour hadron production in proton–nucleus collisions allow for an assessment of the various effects related to the presence of nuclei in the colliding system, denoted as cold-nuclear-matter (CNM) effects. Heavy quarks (charm and beauty) are primarily produced in hard-scattering processes with large momentum transfer (Q^2) due to their large masses. Their inclusive production cross sections can therefore be calculated perturbatively in Quantum Chromodynamics (QCD) utilizing the factorisation approach. In this scheme, the p_{T} differential production cross sections of hadrons containing charm or beauty quarks are calculated as a convolution of three terms: (i) the parton distribution functions (PDFs) of the incoming nucleons, (ii) the partonic scattering cross section, calculated as a perturbative series in powers of the strong coupling constant α_{s}, and (iii) the fragmentation function, which parametrises the non-perturbative evolution of a heavy quark into a given heavy-flavour hadron species. Theoretical predictions based on perturbative QCD (pQCD) calculations at next-to-leading order accuracy with all-order resummation of next-to-leading logarithms, such as FONLL [1, 2] and GM-VFNS [3–6],

can describe within uncertainties the production cross sections of D and B mesons measured in pp and p$\bar{\text{p}}$ collisions in different kinematic regions at centre-of-mass energies from 0.2 to 13 TeV (see e.g. refs. [7, 8] and references therein). In proton–nucleus collisions, various effects in the initial and final state could modify the D-meson production cross sections per nucleon–nucleon collision as compared to pp interactions. In the initial state, the production is affected by the modification of the PDFs in bound nucleons compared to those of free nucleons, depending on the parton momentum fraction x, the momentum transfer Q^2 in the hard scattering process, and the nucleus mass number A [9, 10]. At LHC energies and at mid-rapidity, the most relevant effect on the PDFs is shadowing: a reduction of the parton densities at low x (below 10^{-2}), which becomes stronger when Q^2 decreases and the nucleus mass number A increases. This effect can be described by means of phenomenological parametrisations of the PDF modifications, denoted as nuclear PDFs (nPDFs) [11–14]. As demonstrated in refs. [15, 16], measurements of heavy-flavour and quarkonium production at the LHC can significantly reduce the uncertainties on the gluon nPDFs at small x. If the parton phase-space reaches saturation, the appropriate theoretical description is the Colour Glass Condensate effective theory (CGC) [17–21]. The modification of the small-x parton dynamics can significantly reduce the D-meson yield at low p_{T}. Furthermore, the multiple scattering of partons in the nucleus, before and/or after the hard scattering, can modify the kinematic distribution of the produced hadrons. Partons can lose energy in the initial stages of the collision via initial-state radiation [22], or experience transverse momentum broadening due to multiple soft collisions before the heavy-quark pair is produced [23–25]. These effects can also induce a significant modification of D-meson production at low p_{T}. In addition, final-state effects may also be responsible for a modification of heavy-flavour hadron yields and momentum distributions. The presence of significant final-state effects in p–Pb collisions with large multiplicities of produced particles is suggested by different observations, e.g. the presence of long-range structures in two-particle angular correlations of charged hadrons [26–31], the studies of azimuthal anisotropies in multi-particle correlations [32, 33], the evolution with multiplicity of the identified-hadron transverse-momentum distributions [34, 35], and the suppression of the $\psi(2\text{S})$ production with respect to that of J/ψ mesons [36–38]. In particular, the angular correlations in high-multiplicity p–Pb collisions were found to have similar properties (e.g. particle mass and p_{T} dependence [34, 35]) as those observed in Pb–Pb collisions, where they are commonly interpreted as indications of a collective particle flow produced during the hydrodynamic evolution of the Quark-Gluon Plasma (QGP) [39–42]. The interpretation of the aforementioned results is highly debated, with the outstanding open question being whether small droplets of a fluid-like QGP are created in small collision systems (see e.g. [43] for a recent review). Hydrodynamic calculations, that assume the formation of a medium with some degree of collectivity (see e.g. [44–46]), can describe the angular correlations measured in p–Pb collisions, which suggests a common hydrodynamic origin of the experimental observations from small to large collision systems. However, alternative explanations exist, based on gluon saturation (CGC) in the initial state [47, 48], the anisotropic escape probability of partons from the collision zone [49], or interactions between string-like colour fields in dense configurations of confined QCD flux

tubes [50, 51]. If a collective expansion in the final state of the collision occurs, the medium could also impart a flow to heavy-flavour quarks or hadrons, and modify the hadronisation dynamics of heavy quarks. Detailed calculations were performed in the framework of transport models, assuming that in p–Pb collisions at LHC energies a QGP is formed, which affects the propagation and hadronisation of heavy quarks [52, 53]. These models predict a significant modification of the p_T distributions of heavy-flavour hadrons in high-multiplicity p–Pb collisions as compared to pp interactions, accompanied by the presence of anisotropies in their azimuthal distributions. Recent measurements of angular correlations in p–Pb collisions involving J/ψ mesons [54], D^0 mesons [55], and heavy-flavour decay electrons [56] provided a clear indication that long-range anisotropies are present also in the heavy-flavour sector.

In the presence of a QGP, a modification of the hadronisation is predicted: hadrons can be produced not only via the fragmentation mechanism, but also via (re)combination of charm quarks with other quarks from the medium during the deconfined phase or at the phase boundary [57–60]. Given the observed increase of strangeness production with increasing particle multiplicity in p–Pb and pp collisions [34, 61, 62], the modified hadronisation could result in an enhancement of the relative yield of D_s^+ mesons with respect to non-strange charmed mesons in high-multiplicity p–Pb collisions.

In this paper, we report the measurements of the p_T-differential production cross sections and nuclear modification factors of prompt D^0, D^+, D^{*+}, and D_s^+ mesons in p–Pb collisions at $\sqrt{s_{NN}} = 5.02$ TeV recorded with the ALICE detector in 2016. The sample used for these analyses is larger by a factor of about six with respect to the sample collected in 2013, which was used in previous publications of these observables [63–65]. Therefore, it is possible to obtain lower statistical and systematic uncertainties by a factor 1.5–2 and extend the p_T reach of the measurements. The ratios of the production cross sections of the different D-meson species are also reported and are compared with those measured in pp collisions at the same centre-of-mass energy. The nuclear modification factor, R_{pPb}, is defined as the ratio of the cross section in p–Pb collisions to that in pp interactions scaled by the mass number of the Pb nucleus. This ratio is sensitive to cold-nuclear-matter and hot-medium effects on D-meson production in p–Pb collisions. In addition, the measurement of the nuclear modification factor for non-strange D mesons is carried out in intervals of collision centrality, called in the following as Q_{pPb}. The Q_{pPb} is calculated as the ratio of the D-meson yield in p–Pb collisions to the cross section in pp interactions scaled by the nuclear overlap function $\langle T_{pPb} \rangle$, which accounts for the average number of nucleon-nucleon interactions in the considered centrality class. The Q_{pPb} measurements are performed in finer intervals of collision centrality, enabling in particular the measurements of D-meson production in the 10% most central collisions, in which possible final-state effects are expected to be stronger. Further insight into the centrality dependence of prompt D-meson p_T distributions is provided by the measurements of the ratios of D-meson yields in various centrality classes. Finally, the ratio of D_s^+-meson yield to that of non-strange D^+ is presented as a function of the multiplicity of charged particles produced in p–Pb collisions and is compared with results measured in pp and Pb–Pb collisions at the same centre-of-mass energy.

2 Experimental apparatus and data sample

The ALICE apparatus [66] is composed of a central barrel comprising various detectors for particle reconstruction and identification at mid-rapidity ($|\eta| < 0.9$), a forward muon spectrometer ($-4 < \eta < -2.5$), and a set of forward-backward detectors for triggering and event characterisation. Typical detector performance in pp, p–Pb, and Pb–Pb collisions is presented in [67]. The main detector components used in this analysis are the V0 detector, the Inner Tracking System (ITS), the Time Projection Chamber (TPC), and the Time-Of-Flight (TOF) detector, which are located inside a large solenoidal magnet providing a maximum uniform magnetic field of 0.5 T parallel to the LHC beam direction (z-axis in the ALICE reference system), and the Zero-Degree Calorimeter (ZDC), located at ± 112.5 m from the interaction point.

Proton–lead collisions at $\sqrt{s_{\mathrm{NN}}} = 5.02$ TeV were recorded with a minimum-bias (MB) interaction trigger that required coincident signals in both scintillator arrays of the V0 detector, which cover the full azimuth in the pseudorapidity intervals $-3.7 < \eta < -1.7$ and $2.8 < \eta < 5.1$. The V0 timing information was used together with that from the ZDCs for offline rejection of beam–beam or beam–gas interactions happening outside of the nominal colliding bunches.

The MB trigger was sensitive to about 96.4% of the p–Pb inelastic cross section [68]. Only collision events with a primary vertex reconstructed within ± 10 cm from the centre of the detector along the beam axis were considered. Events with several interactions per bunch crossing, whose probability was below 0.5%, were rejected using an algorithm based on track segments, defined within the Silicon Pixel Detector (SPD, the two innermost ITS layers), to detect multiple interaction vertices.

The number of events passing these selection criteria was about 6×10^8. The corresponding integrated luminosity, $L_{\mathrm{int}} = N_{\mathrm{MB}}/\sigma_{\mathrm{MB}}$, is equal to $292 \pm 11~\mu\mathrm{b}^{-1}$, $\sigma_{\mathrm{MB}} = 2.09$ b being the MB-trigger (i.e. visible) cross section measured via a van der Meer scan, with negligible statistical uncertainty and a systematic uncertainty of 3.7% [68]. During the p–Pb data-taking period, the beam energies were 4 TeV for protons and 1.58 TeV per nucleon for lead nuclei. With this beam configuration, the nucleon–nucleon centre-of-mass system moves in rapidity by $\Delta y_{\mathrm{cms}} = 0.465$ in the direction of the proton beam. The D-meson analyses were performed in the laboratory-frame interval $|y_{\mathrm{lab}}| < 0.5$, which leads to a shifted centre-of-mass rapidity coverage of $-0.96 < y_{\mathrm{cms}} < 0.04$. Additionally, the p–Pb data sample was divided into centrality classes defined as percentiles of the visible cross section. The events were classified according to the energy deposited in the ZDC positioned in the Pb-going side by the neutrons produced in the interaction by nuclear de-excitation processes, or knocked out by wounded nucleons. The multiplicity of these neutrons is expected to grow monotonically with the number of nucleon–nucleon binary collisions, N_{coll}. It was demonstrated in ref. [69] that this is the least-biased centrality estimator for p–Pb interactions. The description of the average nuclear overlap function, as well as the values corresponding to the measured centrality classes, will be given in section 5.3.

The pp reference for the R_{pPb} and Q_{pPb} calculation was taken from the measurements performed on a data sample of about 990 million minimum-bias pp collisions ($L_{\mathrm{int}} = (19.3 \pm 0.4)$ nb^{-1}) at $\sqrt{s} = 5.02$ TeV collected with ALICE in 2017, and published in ref. [70].

3 Data analysis

The D-meson yields were extracted using two different analysis methods. The first method, described in section 3.1, is based on the reconstruction of decay vertices displaced from the primary vertex. The second method, described in section 3.2, is used only for the D^0 measurement and is based on the estimation and subtraction of the combinatorial background, without any selection criteria on the displaced decay-vertex topology. The first method allows the D-meson yield to be extracted in a p_{T}-interval of 1–36 GeV/c for D^0, D^+, and D^{*+} and 2–24 GeV/c for D_s^+. The second method allows the D^0-meson production to be measured down to $p_{\mathrm{T}} = 0$.

3.1 Analysis with D-meson decay vertex reconstruction

The D mesons and their charge conjugates were reconstructed in the decay channels $D^0 \to K^-\pi^+$ (with a branching ratio, BR, of $3.89 \pm 0.04\%$), $D^+ \to K^-\pi^+\pi^+$ (BR of $8.98 \pm 0.28\%$), $D^{*+} \to D^0\pi^+$ (BR of $67.7 \pm 0.5\%$), and $D_s^+ \to \phi\pi^+$ (with $\phi \to K^+K^-$) (BR of $2.27 \pm 0.08\%$) [71]. The analyses were based on the reconstruction of decay vertices displaced from the interaction vertex, exploiting the separation of a few hundred microns induced by the weak decays of the D^0, D^+, and D_s^+ mesons. The displacement of the D^0-meson candidate decay vertex was used to select the D^{*+} meson which decays strongly at the primary vertex. This is performed by combining the D^0 candidates with a soft pion in an invariant-mass analysis.

The D^0, D^+, and D_s^+ candidates were defined using pairs or triplets of tracks with proper charge sign combinations with $|\eta| < 0.8$, $p_{\mathrm{T}} > 0.3$ GeV/c, at least 70 associated space points in the TPC, and at least two space points in the ITS, with at least one in the SPD. The D^{*+} candidates were formed by combining D^0 candidates with tracks satisfying $|\eta| < 0.8$, $p_{\mathrm{T}} > 0.1$ GeV/c and at least two space points in the ITS, including at least one in the SPD. The selection of tracks with $|\eta| < 0.8$ limits the D-meson acceptance in rapidity, which, depending on p_{T}, varies from $|y_{\mathrm{lab}}| < 0.5$ at low p_{T} to $|y_{\mathrm{lab}}| < 0.8$ at $p_{\mathrm{T}} > 5$ GeV/c [72]. A p_{T}-dependent fiducial acceptance region was therefore defined as $y_{\mathrm{fid}}(p_{\mathrm{T}}) > |y_{\mathrm{lab}}|$, with $y_{\mathrm{fid}}(p_{\mathrm{T}})$ increasing from 0.5 to 0.8 in the transverse momentum range $0 < p_{\mathrm{T}} < 5$ GeV/c according to a second-order polynomial function, and $y_{\mathrm{fid}} = 0.8$ for $p_{\mathrm{T}} > 5$ GeV/c. The selection strategy is the same as in previous analyses [65]. The main variables used to select the D-meson candidates are the separation between primary and secondary vertex, the displacement of the tracks from the primary vertex, and the pointing of the reconstructed D-meson momentum to the primary vertex. For the D^+, a selection on the impact parameter of the candidate with respect to the primary vertex in the transverse plane was also applied. For the D_s^+-candidate selection, one of the two pairs of opposite-sign tracks is required to have a reconstructed K^+K^- invariant mass compatible with the

PDG world average of the ϕ meson mass [71]. Further background reduction is achieved by applying particle identification to select charged pions and kaons using information of the TPC and TOF detectors. The track particle identification (PID) is obtained using a 3σ window around the expected mean values of the specific ionisation energy loss ($\mathrm{d}E/\mathrm{d}x$) in the TPC gas and of the time of flight from the interaction point to the TOF detector. A 2σ window around the expected mean values of the $\mathrm{d}E/\mathrm{d}x$ was applied, except for the lowest p_T interval, $1.5 < p_\mathrm{T} < 2$ GeV/c, D^{*+} meson, and for the $\mathrm{D_s^+}$ meson in those cases in which no time-of-flight information was available.

The D-meson raw yields were obtained by fitting the candidate invariant-mass distributions for each D-meson species and the mass difference $\Delta M = M_{\mathrm{K}\pi\pi} - M_{\mathrm{K}\pi}$ for D^{*+}. Examples of these distributions are shown in figure 1 for D^0, D^+, D^{*+}, and $\mathrm{D_s^+}$ mesons in different p_T intervals. The D^0, D^+, and $\mathrm{D_s^+}$ candidate invariant-mass distributions were fit with a function composed of a Gaussian for the signal shape and an exponential term to describe the background shape. The ΔM distribution of the D^{*+} candidates was fit with a Gaussian function for the signal shape and a threshold function multiplied by an exponential for the background: $a\sqrt{\Delta M - m_\pi} \cdot \mathrm{e}^{b(\Delta M - m_\pi)}$, where a and b are free parameters. To account for the contribution of signal candidates that are present in the invariant-mass distribution of the D^0 meson but were assigned the wrong decay-particle mass (reflections) an additional term was included in the fit function. The contribution of the reflections was modelled with a double Gaussian function parametrised on their invariant-mass distributions from Monte Carlo simulations.

For the $M_{\mathrm{KK}\pi}$ distribution, an additional Gaussian was used to describe the $\mathrm{D}^+ \to \mathrm{K}^+\mathrm{K}^-\pi^+$ signal peak present on the left side of the $\mathrm{D_s^+}$ signal. The extracted signal is denoted as S and the background level under the signal peak is denoted as B. The statistical significance of the observed signals, here defined as $(S/\sqrt{S+B})$, varies from 3 to 62, depending on the meson species, the centrality and the p_T interval.

The D-meson raw yields extracted in each p_T interval were corrected to obtain the prompt D-meson cross sections according to

$$\frac{\mathrm{d}^2\sigma^{\mathrm{prompt\,D}}}{\mathrm{d}p_\mathrm{T}\mathrm{d}y} = \frac{1}{\Delta p_\mathrm{T}} \cdot \frac{f_{\mathrm{prompt}}(p_\mathrm{T}) \cdot \frac{1}{2} \cdot N^{\mathrm{D}+\overline{\mathrm{D}},\mathrm{raw}}(p_\mathrm{T})}{c_{\Delta y}(p_\mathrm{T})} \cdot \frac{1}{(\mathrm{Acc}\times\epsilon)_{\mathrm{prompt}}(p_\mathrm{T})} \cdot \frac{1}{\mathrm{BR}\cdot L_{\mathrm{int}}} \,. \quad (3.1)$$

In the formula, $N^{\mathrm{D}+\overline{\mathrm{D}},\mathrm{raw}}$ is the raw yield (sum of particles and antiparticles) in the laboratory rapidity interval $|y_{\mathrm{lab}}| < y_{\mathrm{fid}}(p_\mathrm{T})$ in a p_T interval of width Δp_T. The raw yield includes contributions from prompt and non-prompt D mesons. Non-prompt D mesons originating from beauty-hadron decays are labeled as 'feed-down' in the following. The f_{prompt} term is the fraction of prompt D mesons in the raw yield. The rapidity acceptance correction factor $c_{\Delta y}$ was computed using the PYTHIA v6.4.21 event generator [73] with the Perugia-2011 tune as the ratio between the generated D-meson yield in $\Delta y = 2\,y_{\mathrm{fid}}$, and that in $|y_{\mathrm{lab}}| < 0.5$. The $c_{\Delta y}$ correction factor has a uniform D-meson rapidity distribution in $|y_{\mathrm{lab}}| < y_{\mathrm{fid}}$ in the range $|y_{\mathrm{lab}}| < 0.8$ as shown in [65]. The factor $1/2$ accounts for the fact that the measured yields include particles and antiparticles while the cross sections are given for particles only. The $(\mathrm{Acc}\times\epsilon)_{\mathrm{prompt}}$ is the product of the acceptance of the detectors
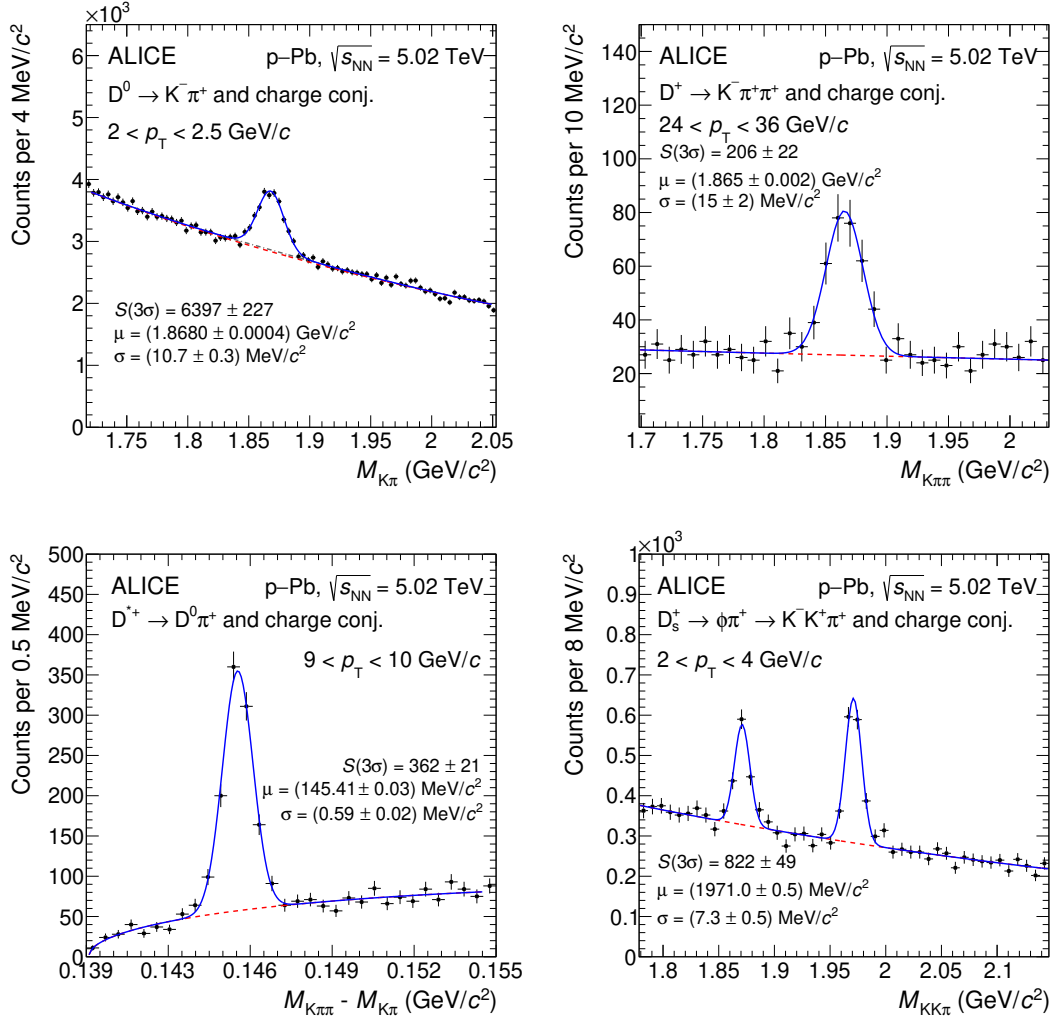
Figure 1. Examplary invariant-mass distributions for D^0, D^+, and D_s^+ candidates (plus charge conjugates) and the mass difference $\Delta M = M_{K\pi\pi} - M_{K\pi}$ for D^{*+} candidates (and charge conjugates) in minimum-bias p–Pb collisions at $\sqrt{s_{NN}} = 5.02$ TeV. The dashed curves represent the fit applied to the background, while the solid lines represent the total fit function. In the case of the D^0 meson, the contribution of signal reflections in the invariant-mass distribution is shown using a gray dot-dashed line. In the case of the D_s^+ invariant-mass distribution, an additional Gaussian is used in the fit function in order to describe the D^+ signal peak on the left side of the D_s^+ signal.

and the efficiency of prompt D mesons, where ϵ accounts for primary vertex reconstruction, D-meson decay track reconstruction and selection, as well as for D-meson candidate selection efficiencies. Finally, BR is the branching ratio of the considered decay channel.

The acceptance and the efficiency were obtained by means of Monte Carlo simulations, that include a detailed description of the apparatus geometry, the detector response, as well as the LHC beam conditions. Proton–proton collisions requiring a $c\bar{c}$ or $b\bar{b}$ pair satisfying $|y| < 1$ were generated using a PYTHIA v6.4.21 event generator [73] with the Perugia-2011 tune. An underlying p–Pb collision, generated with HIJING 1.36 [74], was superimposed
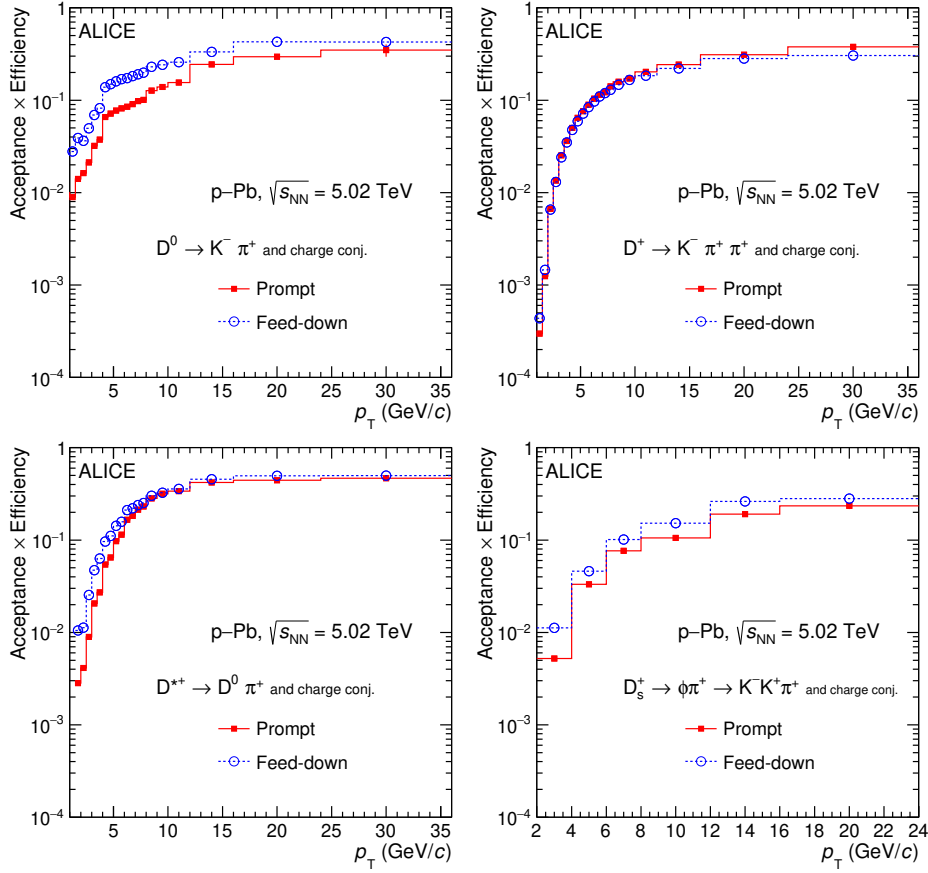
Figure 2. The product of acceptance and efficiency for D^0, D^+, D^{*+}, and D_s^+ mesons as a function of transverse momentum in p–Pb collisions at $\sqrt{s_{NN}} = 5.02$ TeV. The values for prompt (solid line) and feed-down (dashed line) D mesons are shown.

to each PYTHIA event in order to describe the charged-particle multiplicity and detector occupancy observed in data. To reproduce the primary vertex resolution found in data which improves with increasing multiplicity, generated events were weighted on the basis of their charged particle multiplicity. The shape of the generated D-meson p_T distribution is consistent with that of FONLL pQCD calculations [1] at $\sqrt{s} = 5.02$ TeV. The results from FONLL calculations are found to be consistent with pp data at $\sqrt{s} = 5.02$ TeV though at upper edge of uncertainties as described in [70].

Figure 2 shows the product of acceptance and efficiency (Acc × ε) for prompt and feed-down D mesons with rapidity $|y_{lab}| < y_{fid}(p_T)$. The D^0, D^{*+}, and D_s^+ distributions are overall higher for the feed-down contribution compared to that of the prompt D mesons, while the opposite is true for the D^+ efficiency because of the topological selection.

The correction factor f_{prompt} was calculated per p_T interval using a FONLL-based method as described in [75]. The procedure uses the B-meson production cross section in pp collisions at $\sqrt{s} = 5.02$ TeV estimated utilising FONLL calculations, the $B \rightarrow D + X$ decay kinematics from the EvtGen package [76], the efficiencies for D mesons from beauty-hadron decays and a hypothesis on the nuclear modification factor $R_{pPb}^{feed-down}$ of D mesons from B

decays. The $R_{\rm pPb}$ of prompt and feed-down D mesons were assumed to be equal on the basis of calculations including initial-state effects via the EPS09 nPDF parametrisations [11] or the Colour Glass Condensate formalism [21], as well as the measurements of the B^0-meson production in p–Pb collisions at $\sqrt{s_{\rm NN}} = 5.02$ TeV published by the CMS Collaboration [77]. Further details are given in section 4. The resulting $f_{\rm prompt}$ values vary between 0.8 to 0.96 in the $|y_{\rm lab}| < y_{\rm fid}(p_{\rm T})$ interval depending on the $p_{\rm T}$ range and the D-meson species.

3.2   Analysis without D-meson decay-vertex reconstruction

In order to extend the cross section measurement down to $p_{\rm T} = 0$, a different analysis method, which does not employ geometrical selections on the displaced decay-vertex topology, was utilized for the two-body decay $D^0 \to K^-\pi^+$ (and its charge conjugate) [65]. This analysis technique is based on particle identification and on the estimation and subtraction of the combinatorial background of Kπ pairs. Tracks with $|\eta| < 0.8$ and $p_{\rm T} > 0.4$ GeV/c were selected by applying the same track-quality cuts and pion and kaon identification criteria described above for the analysis with decay-vertex reconstruction. The D^0 and $\overline{\rm D}^0$ candidates were formed by combining kaon and pion tracks with opposite charge sign (UnLike Sign, ULS). The resulting candidates were selected by applying the $p_{\rm T}$-dependent fiducial acceptance selection, $|y_{\rm lab}| < y_{\rm fid}(p_{\rm T})$, adopted for the analyses with decay-vertex reconstruction. No selections based on secondary-vertex displacement were applied because at very low $p_{\rm T}$ the D-meson decay topology cannot be efficiently resolved due to the insufficient resolution of the track impact parameter and the small Lorentz boost. The combinatorial background was estimated with the track-rotation technique. For each D^0 (and $\overline{\rm D}^0$) candidate, up to 19 combinatorial-background-like candidates were created by rotating the kaon track by different angles in the range between $\frac{\pi}{10}$ and $\frac{19\pi}{10}$ radians in azimuth. The invariant-mass distribution of ULS Kπ pairs in the transverse momentum interval $0 < p_{\rm T} < 1$ GeV/c is shown in the left panel of figure 3 together with the one of the background estimated with the track-rotation technique, which was normalised to match the yield of ULS pairs at one edge of the invariant-mass interval considered for the extraction of the D^0 signal.

The invariant-mass distribution of background candidates was subtracted from the one of ULS Kπ pairs and the resulting distribution, which contains the D^0 signal and the remaining background, is shown in the right panel of figure 3. The D^0-meson raw signal (sum of particle and antiparticle contributions) was extracted via a fit to the background-subtracted invariant-mass distribution. The fit function is composed of a Gaussian term to describe the signal, a second-order polynomial function to model the remaining background, and a term describing the contribution of signal candidates passing the selection criteria with swapped mass hypotheses of the final-state kaon and pion (reflections), whose invariant-mass distribution was taken from simulation. The signal-to-background ratio increases from $6 \cdot 10^{-4}$ to $3 \cdot 10^{-2}$ with increasing $p_{\rm T}$ and the statistical significance is about 9 in $0 < p_{\rm T} < 1$ GeV/c and is greater than 15 for $p_{\rm T} > 2$ GeV/c.

The acceptance and efficiency were determined from the same Monte Carlo simulations used for the analysis with decay-vertex reconstruction. The resulting (Acc × ϵ) of prompt D^0 mesons is shown as a function of $p_{\rm T}$ in figure 4. Compared to the analysis with decay-
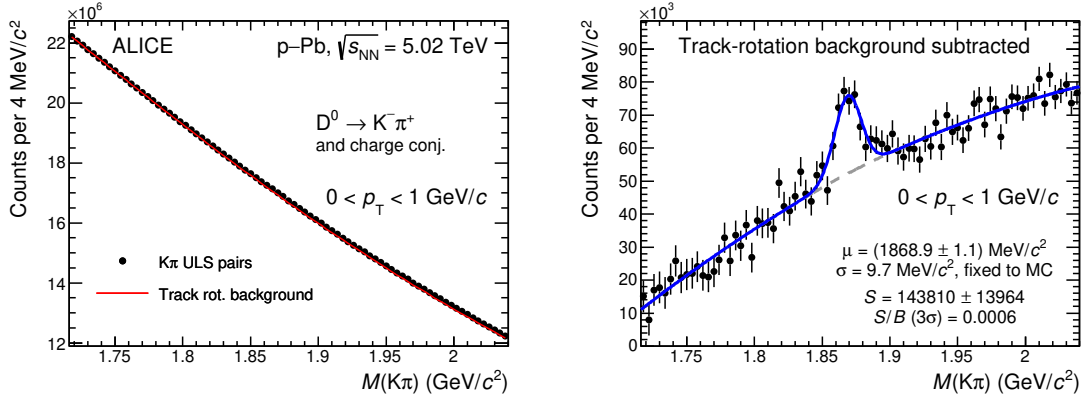
Figure 3. Invariant-mass distributions of $D^0 \to K^-\pi^+$ candidates (and charge conjugates) for $0 < p_T < 1$ GeV/c. The left panel displays the invariant-mass distribution of all ULS $K\pi$ pairs together with the background distribution estimated with the track-rotation technique. The right panel shows the invariant-mass distribution after subtracting the background estimated with the track-rotation technique. The fit function is superimposed.
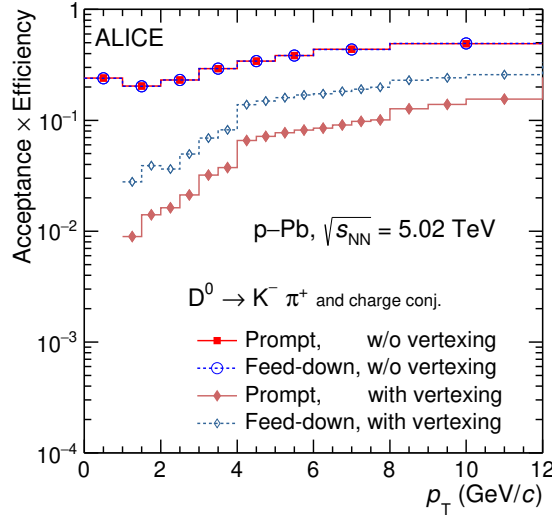
Figure 4. Product of acceptance and efficiency of $D^0 \to K^-\pi^+$ (and charge conjugates) in p–Pb collisions for the analyses with and without reconstruction of decay vertex.

vertex reconstruction, the efficiency is higher by a factor of about 20 (3) at low (high) p_T and it demonstrates a less steep p_T dependence. Note that for the analysis without decay-vertex reconstruction the efficiency ϵ is almost independent of p_T and the increase of the (Acc $\times$ ϵ) with increasing p_T is mainly determined by the geometrical acceptance of the apparatus. Unlike in the analysis with decay-vertex reconstruction, the efficiency is the same for prompt D^0 mesons and D^0 mesons from beauty-hadron decays.

The prompt contribution to the D^0-meson raw yield, f_{prompt}, was estimated with the same FONLL-based method used for the analysis with decay-vertex reconstruction. The resulting f_{prompt} values decrease with increasing p_T (from about 0.96 for $p_T < 3$ GeV/c

to about 0.9 in the interval $8 < p_T < 12$ GeV/c) and are larger than in the analysis with decay-vertex reconstruction, since the feed-down component is not enhanced by the selection criteria.

3.3 Measurement of the prompt D-meson fraction based on a data-driven method

The prompt fractions of D^0, D^+, and D^{*+} mesons, calculated via the FONLL-based method, were cross-checked for the analysis with decay vertex reconstruction utilizing a data-driven method that exploits the different shapes of the transverse-plane impact parameter to the primary vertex (d_0) of prompt and feed-down D mesons. The D-meson candidates were selected using the same criteria described in section 3.1, with the exception that for D^+ the impact-parameter selection criteria were not applied. An additional selection was based on the candidate invariant-mass fits. The D^0 and D^+ mesons candidates were selected to have an invariant mass $|M - M_D| < 1.5\sigma$, while for D^{*+}-meson candidates a $|\Delta M - \Delta M_{D^{*+}}| < 2.5\sigma$ selection was applied, where σ is the standard deviation of the Gaussian function describing the D-meson invariant-mass signal. The prompt fraction was estimated via an unbinned likelihood fit of the d_0 distribution of the D-meson candidates using the fit function

$$F(d_0) = S \cdot \left[(1 - f_{\text{prompt}}) F^{\text{feed-down}}(d_0) + f_{\text{prompt}} F^{\text{prompt}}(d_0) \right] + B \cdot F^{\text{backgr}}(d_0). \quad (3.2)$$

In this function, $F^{\text{prompt}}(d_0)$, $F^{\text{feed-down}}(d_0)$ and $F^{\text{backgr}}(d_0)$ are functions describing the impact-parameter distributions of prompt and feed-down D mesons and of background candidates. The function F^{prompt} consists of a detector resolution term modeled with a Gaussian function and a symmetric exponential term, $\frac{1}{2\lambda} \exp\left(-\frac{|d_0|}{\lambda}\right)$ (with λ as a free parameter), with the latter describing the tails of the impact-parameter distribution of prompt D mesons. The $F^{\text{feed-down}}$ is the convolution of the detector resolution term with a symmetric double-exponential function ($F^{\text{feed-down}}_{\text{true}}$) that describes the intrinsic impact-parameter distribution of D mesons from B-meson decays, which is determined by the decay length and decay kinematics of B mesons. The parameters of the F^{prompt} and $F^{\text{feed-down}}_{\text{true}}$ functions were fixed to the values obtained by fitting the distributions from Monte Carlo simulations, with the exception of the Gaussian width of the detector-resolution term, which was kept free when applying the fit to the data in order to compensate for a possible imperfect description of the impact-parameter resolution in the simulation. The function F^{backgr} was parametrised on the impact-parameter distribution of background candidates, which were selected from side bands relative to the signal peak in the invariant-mass distributions, and in the case of D^{*+}, the mass-difference distribution. The function consists of a double Gaussian and a symmetric exponential term, which describes the tails, as reported in ref. [65]. In the case of the D^+, the function presents a double-peak structure with a depletion around zero that is induced by the selections applied.

The left panels of figure 5 show examples of fits to the impact-parameter distributions of D^0, D^+, and D^{*+} mesons in the transverse-momentum intervals $2 < p_T < 3$ GeV/c, $3 < p_T < 4$ GeV/c, and $5 < p_T < 6$ GeV/c, respectively. The prompt fraction estimated using
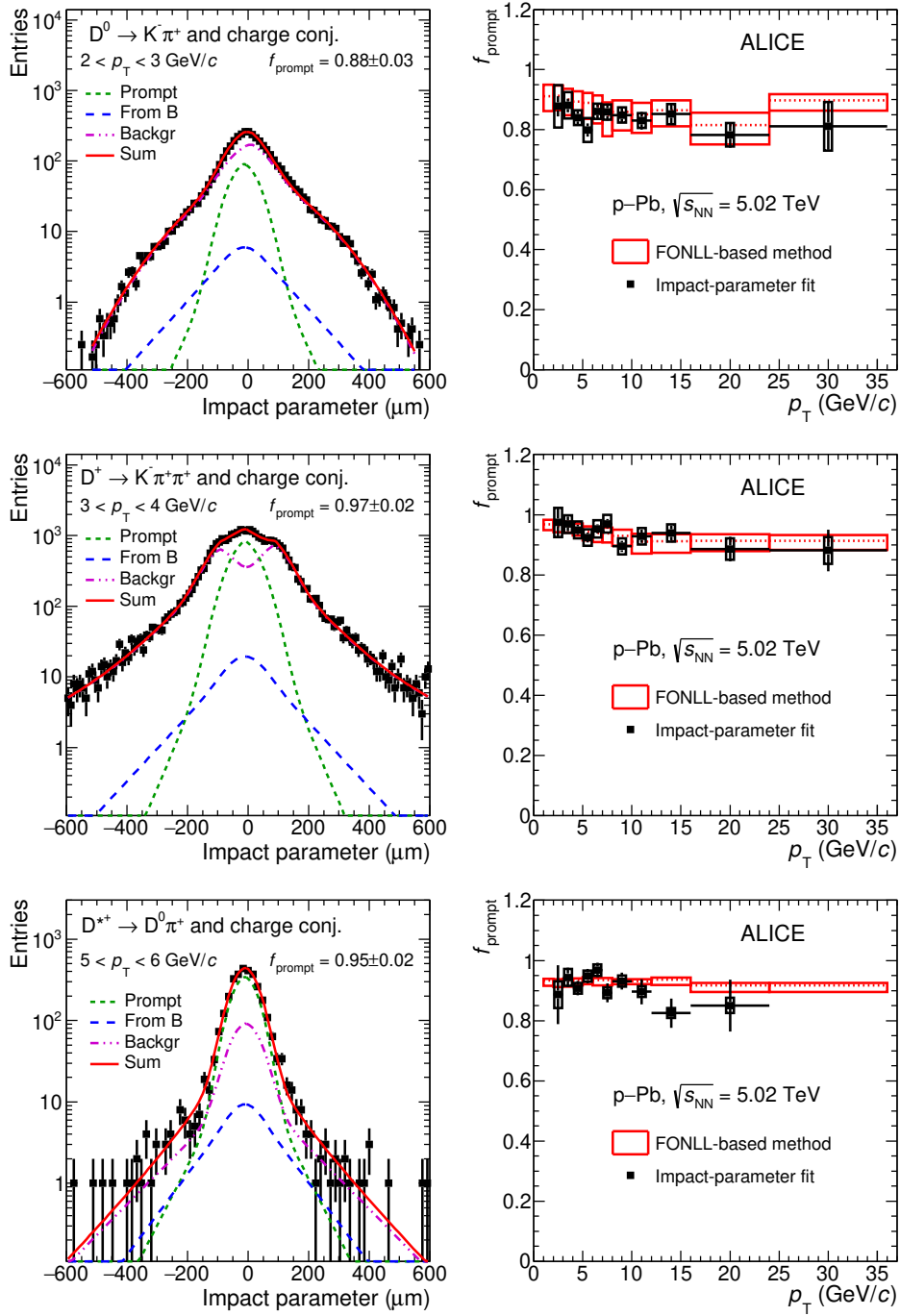
Figure 5. Left: Exemplary fits to the impact-parameter distributions of D^0, D^+, and D^{*+} candidates. The curves show the fit functions describing the prompt, feed-down, and background contributions as well as their sum, as described in the text. Right: fraction of prompt D^0, D^+, and D^{*+} raw yield as a function of transverse momentum p_T compared with the values obtained with the FONLL-based approach. The results from the data-driven method are shown as square markers with the error bars (boxes) representing the statistical (systematic) uncertainty. The central values of f_{prompt} from the FONLL-based approach are shown as the dashed lines and the uncertainty as red boxes.

the data-driven approach has systematic uncertainties due to (i) the impact-parameter distribution assumed for prompt and feed-down D mesons and background candidates; (ii) the uncertainty on the signal and background yields extracted from the invariant-mass fits; and (iii) the consistency of the procedure, evaluated via a Monte Carlo closure test. These uncertainties were estimated using the procedures described in ref. [65]. The total systematic uncertainty on f_{prompt} based on the data-driven approach for the three D-meson species is about 2–3% in the interval $3 < p_{\mathrm{T}} < 16$ GeV/c and about 5% in the interval $2 < p_{\mathrm{T}} < 3$ GeV/c and above 16 GeV/c.

The prompt fraction of D^0, D^+, and D^{*+} mesons measured utilizing the data-driven method is compared with the one calculated with the FONLL-based approach in the right panels of figure 5. For D^0, D^+, and D^{*+} in $1 < p_{\mathrm{T}} < 2$ GeV/c and for the D^{*+} in $24 < p_{\mathrm{T}} < 36$ GeV/c, given the poor precision of the impact-parameter fit, it was not possible to determine f_{prompt} with the data-driven approach. The prompt fraction measured with the impact-parameter fits is compatible with the FONLL-based estimation within 1σ for almost all points.

4 Systematic uncertainties

Systematic uncertainties on the D-meson production cross sections were estimated considering the following sources:
(i) extraction of the raw yield from the invariant-mass distributions; (ii) track reconstruction efficiency; (iii) D-meson selection efficiency; (iv) PID efficiency; (v) the assumption on the shape of the D-meson p_{T} spectrum generated in the simulation; (vi) subtraction of the feed-down from beauty-hadron decays.
In addition, the p_{T}-differential cross sections have a systematic uncertainty on the overall normalisation induced by the uncertainties on the integrated luminosity of 3.7% [68] and on the branching ratios of the considered D-meson decays [71]. The estimated values of the relative systematic uncertainties are summarised in table 1. The contributions of the different sources were summed in quadrature to obtain the total systematic uncertainty.

The systematic uncertainties on the raw yield extraction were evaluated for each D-meson species by repeating the invariant-mass distribution fits, for each p_{T} and centrality interval, varying the lower and upper limits of the fit range and the functional form of the background fit function. In addition, the same approach was used with a bin-counting method, in which the signal yield was obtained by integrating the invariant-mass distribution after subtracting the background estimated from a fit to the side bands. For D^0 mesons, an additional contribution due to the description of signal reflections in the invariant-mass distribution was estimated by varying the ratio of the integral of the reflections over the integral of the signal and the shape of the templates used in the invariant-mass fits. The systematic uncertainty was defined as the root mean square of the distribution of the signal yields obtained from the described variations. The uncertainty ranges between 1% and 15% depending on the D-meson species, p_{T}, event centrality and charged-particle multiplicity intervals of the measurement. An increase in the raw yield extraction uncertainties was observed in the most central collisions due to the lower S/B ratio. For the D^0-meson

p_T (GeV/c)	D^0			D^+		D^{*+}		D_s^+	
	0–1	2–2.5	10–12	2–2.5	10–12	2–2.5	10–12	2–4	8–12
Signal yield ⋄	5%	3%	3%	2%	3%	7%	2%	3%	2%
Tracking efficiency	2.5%	2.5%	2.5%	3.7%	4%	3.2%	4.5%	3.7%	4%
Selection efficiency	negl.	3%	3%	7%	4%	2%	2%	6%	4%
PID efficiency	negl.	negl.	negl.	negl.	negl.	negl.	negl.	1%	1%
p_T shape in MC	negl.	negl.	negl.	negl.	negl.	negl.	negl.	negl.	negl.
Feed-down ⋄	$^{+1.3}_{-1.7}$%	$^{+4.2}_{-4.9}$%	$^{+4.1}_{-5.6}$%	$^{+1.8}_{-2.1}$%	$^{+2.3}_{-3.2}$%	$^{+3.0}_{-3.5}$%	$^{+1.9}_{-2.6}$%	$^{+3.6}_{-4.2}$%	$^{+4.4}_{-5.6}$%
Branching ratio	1.0%			3.1%		1.3%		3.5%	
Normalisation	3.7%								

Table 1. Summary of relative systematic uncertainties on D^0, D^+, D^{*+}, and D_s^+ production cross sections. The event centrality-dependent uncertainties are marked by the symbol ⋄.

analysis without decay-vertex reconstruction, different configurations of the rotation angle were used to estimate the background with the track-rotation technique. Furthermore, three alternative approaches were tested to estimate the background distribution: like-sign (LS) pairs, event mixing, and side-band fit [65]. The raw yield values obtained subtracting these alternative background distributions were found to be consistent with those from the default configuration of the track-rotation method within the uncertainty estimated by varying the fit conditions and therefore no additional systematic uncertainty was assigned. The systematic uncertainty on the track reconstruction efficiency was estimated by varying the track-quality selection criteria and by comparing the probability to match the tracks from the TPC to the hits in the ITS, in the data and simulation. The comparison of the matching efficiency in the data and simulation was made after weighting the relative abundances of primary and secondary particles in the simulation to match those in the data, which were estimated via fits to the track impact-parameter distributions [78]. The estimated uncertainty depends on the D-meson p_T and it ranges from 2.5% to 4% for the two-body decay of D^0 mesons and from 3.7% to 4.5% for the three-body decays of D^+, D^{*+}, and D_s^+ mesons.

The uncertainty on the selection efficiency originates from imperfections in the description of the D-meson kinematic and decay properties and of the detector resolution and alignment in the simulation. For the analyses based on the decay-vertex reconstruction, the uncertainty was estimated by comparing the corrected yields obtained by repeating the analysis with different sets of selection criteria, resulting in a significant modification of efficiencies, raw yield, and background estimates.

The assigned uncertainty for non-strange D mesons is 2–3% in most of the p_T intervals and it increases to 7% at low p_T, where the efficiencies are low and steeply fall with decreasing p_T, because of the tighter geometrical selections. A larger uncertainty (ranging from 7% at high p_T to 14% at low p_T) was estimated for the D_s^+ mesons, for which more stringent selection criteria were used in the analysis, as compared to non-strange D mesons. In the case of the D^0-meson analysis without decay-vertex reconstruction, the stability of

the corrected yield was tested against variations of the single-track p_T selection and no systematic effect was observed.

In addition, the efficiency values could also be sensitive to the generated shapes of the D-meson transverse-momentum distributions and to the multiplicity of particles produced in the collision. The systematic uncertainty due to the generated D-meson p_T spectrum shape was estimated by considering different input distributions (PYTHIA, FONLL) and was found to be negligible. The effect of possible differences between the charged-particle multiplicity distributions in data and multiplicity-weighted simulation, used to compute the efficiencies in the different centrality classes, as explained in section 3.1, varied between 0 and 2% depending on the D-meson species, p_T, event centrality, and charged-particle multiplicity intervals.

To estimate the uncertainty on the PID-selection efficiency the analysis was repeated without PID selection, or with less stringent criteria in the cases where the signal extraction was not reliable without PID, as for example for the D_s^+ and the D^0-meson analysis without decay-vertex reconstruction. In addition, the pion and kaon PID selection efficiencies were compared in the data and in simulation using high purity samples of pions from the decay of K_s^0 and kaons identified with the TOF combined with the D-meson decay kinematics. The PID uncertainty was found to vary between 0 and 1.5% depending on the PID selection criteria used for each D-meson species.

The systematic uncertainty on the subtraction of feed-down from beauty-hadron decays (i.e. the calculation of the f_{prompt} fraction) was estimated by varying the FONLL parameters (b-quark mass, factorisation and renormalisation scales) as described in [2] and by varying the hypothesis on the nuclear modification factor of feed-down D mesons in the range $0.9 < R(Q)_{\mathrm{pPb}}^{\mathrm{feed\text{-}down}}/R(Q)_{\mathrm{pPb}}^{\mathrm{prompt}} < 1.3$ for the integrated centrality interval and central collisions, and between $0.9 < Q_{\mathrm{pPb}}^{\mathrm{feed\text{-}down}}/Q_{\mathrm{pPb}}^{\mathrm{prompt}} < 1.1$ for the peripheral collisions, where the possible differences of the D-meson production mechanisms in p–Pb with respect to pp collisions are expected to be reduced as observed for both charmed mesons and charged particles. The uncertainty ranges between 2% and 5% depending on the D-meson species, p_T, event centrality and charged-particle multiplicity intervals.

5 Results

5.1 p_T-differential cross sections

The analysis without decay-vertex reconstruction allows for a direct measurement of the inclusive D^0-meson cross section because no selections that alter the fraction of prompt and feed-down D mesons are applied. The inclusive D^0-meson cross section in p–Pb collisions is shown in the left panel of figure 6 and is compared with the measurement in pp collisions at the same centre-of-mass energy, published in [70]. The cross section in pp collisions was scaled by the Pb mass number $A = 208$ and corrected for the rapidity shift in p–Pb collisions using FONLL calculations. The correction for the rapidity shift is a p_T-dependent factor of the order of 1–3%. The uncertainty assigned on this correction is evaluated varying the quark mass and the perturbative scale parameters and including the PDFs uncertainty, and is 1% at low p_T and negligible at high p_T.
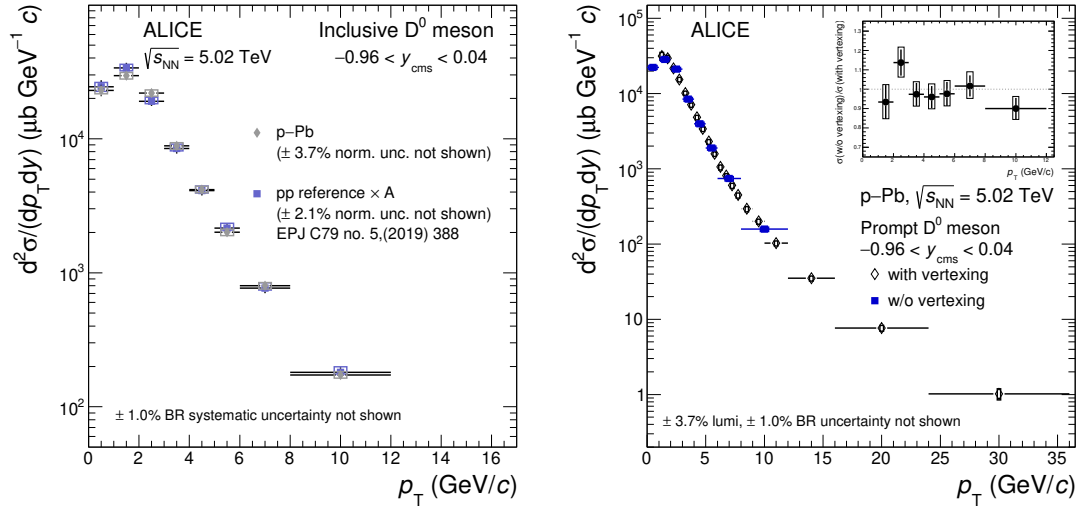
Figure 6. Left: inclusive D^0-meson production cross sections from the analysis without decay-vertex reconstruction in p–Pb collisions and pp collisions, both at $\sqrt{s_{NN}} = 5.02$ TeV. The cross section measured in pp collision [70] is scaled by the Pb mass number ($A = 208$) and corrected for the rapidity shift in p–Pb collisions using FONLL calculations. Right: p_T-differential production cross section of prompt D^0 mesons with $-0.96 < y_{cms} < 0.04$ in p–Pb collisions at $\sqrt{s_{NN}} = 5.02$ TeV, measured with and without decay-vertex reconstruction. The vertical bars and the empty boxes represent the statistical and systematic uncertainties. The inset shows the ratio of the measurements in their common p_T range.

The total cross section for inclusive D^0-meson production in p–Pb collisions per unit of rapidity in $-0.96 < y_{cms} < 0.04$ was obtained by integrating the p_T-differential cross section shown in the left panel of figure 6. The systematic uncertainty was defined by propagating the yield extraction uncertainty as uncorrelated among the p_T intervals and all the other uncertainties as correlated. The cross section was then extrapolated to the whole p_T range using FONLL calculations in order to take into account the fraction of cross section not measured for $p_T > 12$ GeV/c. An uncertainty was estimated for the extrapolation varying the quark mass and the perturbative scale parameters and including the PDFs uncertainty. The resulting cross section is

$$d\sigma^{\text{inclusive}\,D^0}_{\text{p−Pb},\,5.02\,\text{TeV}}/dy = 91.2 \pm 3.4\,(\text{stat.}) \pm 3.2\,(\text{syst.}) \pm 3.4\,(\text{lumi.}) \pm 0.9\,(\text{BR})^{+0.4}_{-0.2}\,(\text{extrap.})\,\text{mb}.$$

(5.1)

The right panel of figure 6 shows the comparison of the p_T-differential production cross sections for prompt D^0 mesons with $-0.96 < y_{cms} < 0.04$ in p–Pb collisions at $\sqrt{s_{NN}} = 5.02$ TeV obtained from the analysis with and without decay-vertex reconstruction. The results are consistent within statistical uncertainties.

Considering the statistical and systematic uncertainties obtained in the two analyses, the most precise measurement of the prompt D^0 production cross section is obtained using the results from the analysis without decay-vertex reconstruction in the interval $0 < p_T < 1$ GeV/c and the analysis with decay-vertex reconstruction for $p_T > 1$ GeV/c. The resulting cross section is shown in the top-left panel of figure 7.
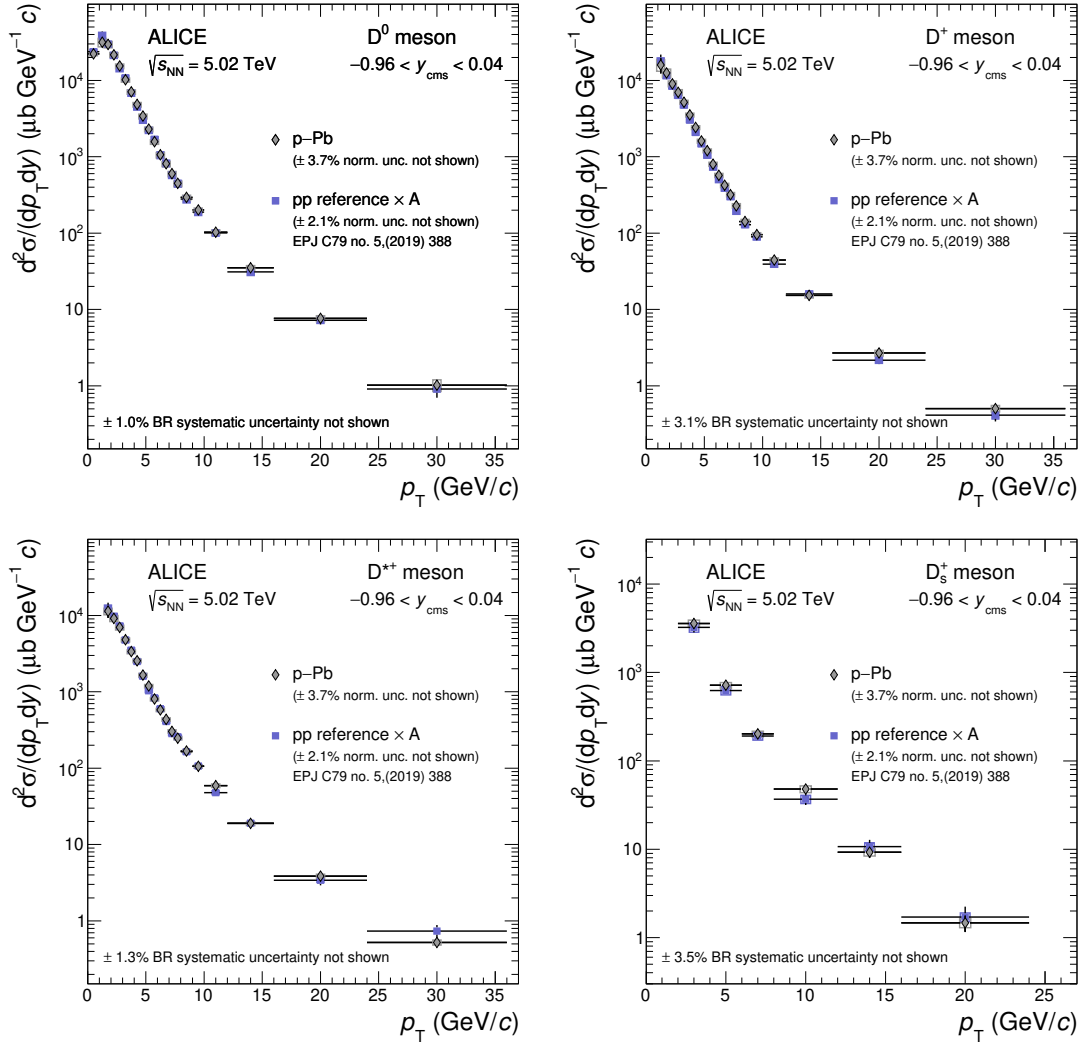
Figure 7. p_{T}-differential production cross sections of prompt D^0, D^+, D^{*+}, and D_s^+ mesons with $-0.96 < y_{\mathrm{cms}} < 0.04$ in p–Pb collisions at $\sqrt{s_{\mathrm{NN}}} = 5.02$ TeV compared with the respective pp reference cross sections [70] scaled by the Pb mass number ($A = 208$) and corrected for the rapidity shift. For the D^0 meson, the results in the range $0 < p_{\mathrm{T}} < 1$ GeV/c are obtained from the analysis that was performed without decay-vertex reconstruction, while those in the range $1 < p_{\mathrm{T}} < 36$ GeV/c are taken from the analysis with decay-vertex reconstruction. The vertical bars and the empty boxes represent the statistical and systematic uncertainties.

The total cross section for prompt D^0-meson production per unit of rapidity in $-0.96 < y_{\mathrm{cms}} < 0.04$ was also calculated by integrating the p_{T}-differential measurement reported in the top-left panel of figure 7, obtained combining the methods with and without decay-vertex reconstruction. The systematic uncertainties were propagated as described above for the total cross section of inclusive D^0 mesons. The resulting value is

$$\mathrm{d}\sigma^{\mathrm{prompt\,D}^0}_{\mathrm{p-Pb,\,5.02\,TeV}}/\mathrm{d}y = 88.5 \pm 2.7\,(\mathrm{stat.})^{+5.3}_{-6.1}\,(\mathrm{syst.}) \pm 3.3\,(\mathrm{lumi.}) \pm 0.9\,(\mathrm{BR})\,\mathrm{mb}. \qquad (5.2)$$

In ref. [65], the $c\bar{c}$ production cross section in the rapidity interval $-0.96 < y_{cms} < 0.04$ was reported. This calculation used the fraction of charm quarks hadronising into D^0 mesons to be $f(c \to D^0) = 0.542 \pm 0.024$ which was derived in ref. [79] by averaging the measurements in e^+e^- collisions at LEP. Recent measurements of the Λ_c-baryon production cross section in pp collisions at $\sqrt{s} = 7$ TeV and in p–Pb collisions at $\sqrt{s_{NN}} = 5.02$ TeV [80, 81] suggest that the fragmentation fractions of charm quarks into charmed baryons in pp collisions at LHC energies might differ significantly from the LEP results. Therefore, more precise measurements of charmed-baryon production cross sections are needed for an accurate calculation of the charm production cross section.

The average transverse momentum $\langle p_T \rangle$ of prompt D^0 mesons was obtained by fitting the cross section reported in the top-left panel of figure 7 with a power-law function $f(p_T) = C\, p_T/(1 + (p_T/p_0)^2)^n$, where C, p_0 and n are the free parameters. The result is:

$$\langle p_T \rangle^{\text{prompt } D^0}_{\text{p–Pb}, 5.02\,\text{TeV}} = 2.07 \pm 0.02\,(\text{stat.}) \pm 0.04\,(\text{syst.})\ \text{GeV}/c, \qquad (5.3)$$

where the systematic uncertainties were estimated with the procedure described in ref. [65]. The result is compatible within statistical uncertainties with the one obtained in pp collisions at the same centre-of-mass energy: $\langle p_T \rangle^{\text{prompt } D^0}_{\text{pp}, 5.02\,\text{TeV}} = 2.06 \pm 0.03\,(\text{stat.}) \pm 0.03\,(\text{syst.})\ \text{GeV}/c$ [70].

The p_T-differential cross sections for the other three D-meson species (D^+, D^{*+}, and D_s^+) are shown in the other panels of figure 7. The cross sections measured in p–Pb collisions are compatible with the measurements published using the 2013 p–Pb data sample [63, 64], while having a factor 1.5–2 smaller statistical and systematic uncertainties and an extended p_T reach. The cross sections in p–Pb collisions are compared with the corresponding pp reference cross sections at the same centre-of-mass energy [70] and rapidity interval.

5.2 The p_T-differential nuclear modification factor

The nuclear modification factor is computed as:

$$R_{\text{pPb}} = \frac{1}{A} \frac{\mathrm{d}^2\sigma^{\text{prompt D}}_{\text{p–Pb}}/\mathrm{d}p_T\mathrm{d}y}{\mathrm{d}^2\sigma^{\text{prompt D}}_{\text{pp}}/\mathrm{d}p_T\mathrm{d}y}, \qquad (5.4)$$

where $\mathrm{d}^2\sigma^{\text{prompt D}}_{\text{p–Pb}}/\mathrm{d}p_T\mathrm{d}y$ is the D-meson p_T-differential cross section in $-0.96 < y_{cms} < 0.04$ in p–Pb collisions at $\sqrt{s_{NN}} = 5.02$ TeV, A is the mass number of the Pb nucleus and $\mathrm{d}^2\sigma^{\text{prompt D}}_{\text{pp}}/\mathrm{d}p_T\mathrm{d}y$ is the cross section in pp collisions at the same centre-of-mass energy from [70] corrected for the rapidity shift in p–Pb collisions. The systematic uncertainties of the p–Pb and pp measurements were considered to be independent and were propagated quadratically, with the exception for the BR uncertainty, which cancels out in the ratio, and the uncertainty on the feed-down correction, which was recalculated for the ratio of cross sections by consistently varying the FONLL calculation parameters in the numerator and the denominator.

Figure 8 shows the nuclear modification factors R_{pPb} of prompt D^0, D^+, and D^{*+} mesons in the left panel and their average, along with the R_{pPb} of D_s^+ mesons, in the right panel.
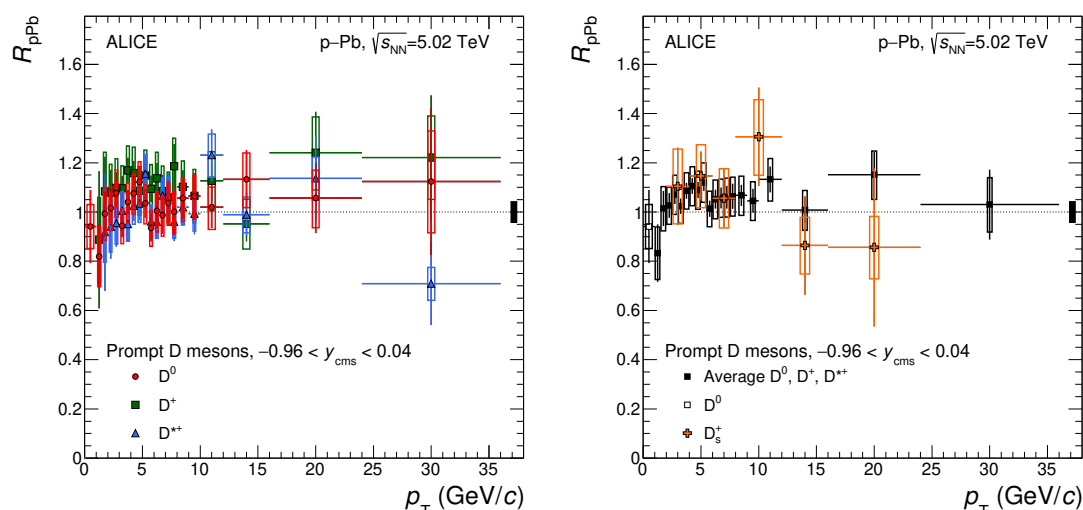
Figure 8. Nuclear modification factors R_{pPb} of prompt D mesons in p–Pb collisions at $\sqrt{s_{NN}} =$ 5.02 TeV. Left: R_{pPb} of D^0, D^+, and D^{*+} mesons. Right: average R_{pPb} of non-strange D-meson species in the interval $1 < p_T < 36$ GeV/c [63], shown together with the D^0 R_{pPb} in $0 < p_T < 1$ GeV/c and the R_{pPb} of D_s^+ mesons in the interval $2 < p_T < 24$ GeV/c. The vertical bars and the empty boxes represent the statistical and systematic uncertainties. The black-filled box at $R_{pPb} = 1$ represents the normalisation uncertainty.

With the current uncertainties it is not possible to disentangle a possible mass dependent effect originating from a collective expansion of the system that would modify the D^{*+} spectrum differently with respect to the D^0 and D^+ spectra. Therefore, the average of the nuclear modification factors of the three non-strange D-meson species is considered and it was calculated using the inverse of the relative statistical uncertainties as weights. The systematic uncertainty of the average was calculated by propagating the uncertainties through the weighted average, while considering the contributions from tracking efficiency and beauty feed-down correction as fully correlated among the three species. The D-meson R_{pPb} is compatible with unity over the entire measured p_T interval within 2 standard deviations. The R_{pPb} of strange and non-strange D mesons are compatible among each other within statistical and systematic uncertainties.

The D-meson nuclear modification factor is also compared with theoretical calculations, shown in figure 9. In the left panel, four theoretical calculations that include only CNM effects are displayed. A calculation based on the Colour Glass Condensate formalism [21, 82] describes the data within a 2σ uncertainty in the entire p_T range, although the model underestimates systematically the measured points at low p_T ($p_T < 6$ GeV/c). A FONLL calculation with CTEQ6M PDFs [83] and EPPS16 NLO nuclear modification [14] is compatible with the data within the uncertainties. The measurement lies on the upper limit of the EPPS16 nPDF uncertainty band, while this is not the case for the D-meson R_{pPb} at forward rapidity measured by LHCb [15, 84]. The data are also described within the uncertainties by a LO pQCD calculation with intrinsic k_T broadening, nuclear shadowing, and energy loss of the charm quarks in cold nuclear matter (Vitev et al.) [85]. The
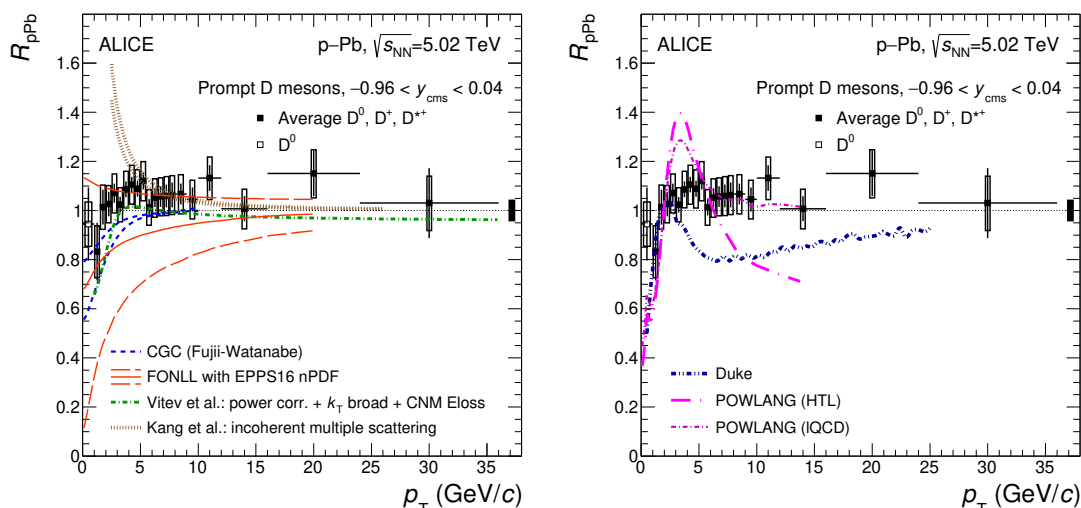
Figure 9. Nuclear modification factor R_{pPb} of prompt non-strange D mesons in p–Pb collisions at $\sqrt{s_{\mathrm{NN}}} = 5.02$ TeV. In the left panel, the data are compared with calculations of theoretical models that include only CNM effects: CGC [82], FONLL [2] with EPPS16 nPDFs [14], a LO pQCD calculation (Vitev et al.) [85], and a calculation based on incoherent multiple scatterings (Kang et al.) [86]. In the right panel, the predictions of the Duke [52] and POWLANG [53] transport models are compared with the measured D-meson R_{pPb}. The vertical bars and the empty boxes represent the statistical and systematic uncertainties. The black-filled box at $R_{\mathrm{pPb}} = 1$ represents the normalisation uncertainty.

calculation by Kang et al., that consists of a higher-twist calculation based on incoherent multiple scatterings, has a different trend with respect to the other models and it is excluded by the data for $p_{\mathrm{T}} < 4$ GeV/c.

In the right panel of figure 9, the measurements are compared with the calculations of two transport models, Duke [52] and POWLANG [53], both of which assume that a QGP is formed in p–Pb collisions. These models are both based on the Langevin approach for the transport of heavy quarks through an expanding deconfined medium described by relativistic viscous hydrodynamics. The Duke model includes both collisional and radiative energy loss. The POWLANG model considers only collisional processes with two choices for the transport coefficients, based on hard-thermal-loop (HTL) and lattice-QCD (lQCD) calculations. For both the Duke and the HTL based POWLANG estimates, the D-meson nuclear modification factor distribution has a peak structure, with the maximum at $p_{\mathrm{T}} \approx 2.5$ GeV/c and $p_{\mathrm{T}} \approx 3.5$ GeV/c, respectively, possibly followed by a moderate ($< 20\text{–}30\%$) suppression at higher p_{T}, resulting from the interplay of CNM effects and interactions of charm quarks with the radially expanding medium. The trend suggested by these models is not supported by the data. The strong enhancement at $p_{\mathrm{T}} \sim 3 - 4$ GeV/c observed in the model calculations is not consistent with the measured R_{pPb}, and a suppression larger than 10% for $p_{\mathrm{T}} > 8$ GeV/c is excluded by the data with a 98% confidence level.

The p_{T}-integrated nuclear modification factor of prompt D^0 mesons in $-0.96 < y_{\mathrm{cms}} < 0.04$ was obtained from eq. (5.4) by integrating the p_{T}-differential cross sections in pp and

Centrality classes	0–10%	10–20%	20–40%	40–60%	60–100%
$\langle T_{\mathrm{pPb}} \rangle$ (1/mb)	0.172	0.158	0.137	0.102	0.046
Rel. unc.	6.9%	3.7%	1.7%	4.8%	5.2%

Table 2. $\langle T_{\mathrm{pPb}} \rangle$ and relative uncertainties for each centrality class considered in the analysis.

p–Pb collisions. The result is

$$R_{\mathrm{pPb}}^{\mathrm{prompt\,D^0}}(p_{\mathrm{T}} > 0, -0.96 < y_{\mathrm{cms}} < 0.04) = 0.96 \pm 0.05\,(\mathrm{stat.})\,^{+0.07}_{-0.07}(\mathrm{syst.}) \qquad (5.5)$$

and it is consistent with the atomic mass number scaling of the total charm cross section.

5.3 The p_{T} and centrality-dependent nuclear modification factor

The measurement of the nuclear modification factor was also computed in various centrality intervals, where the centrality is defined using the energy deposited by neutrons in the ZDC positioned in the Pb-going side (ZN energy), as described in section 2. For each centrality class the nuclear modification factor, Q_{pPb}, is defined as

$$Q_{\mathrm{pPb}} = \frac{(\mathrm{d}^2 N^{\mathrm{prompt\,D}}/\mathrm{d}p_{\mathrm{T}}\mathrm{d}y)^{\mathrm{i}}_{\mathrm{p-Pb}}}{\langle T_{\mathrm{pPb}} \rangle_{\mathrm{i}} \times (\mathrm{d}^2 \sigma_{\mathrm{pp}}^{\mathrm{prompt\,D}}/\mathrm{d}p_{\mathrm{T}}\mathrm{d}y)} \,, \qquad (5.6)$$

where $(\mathrm{d}^2 N^{\mathrm{prompt\,D}}/\mathrm{d}p_{\mathrm{T}}\mathrm{d}y)^{\mathrm{i}}_{\mathrm{p-Pb}}$ is the yield of prompt D mesons in p–Pb collisions and $\langle T_{\mathrm{pPb}} \rangle_{\mathrm{i}}$ is the average nuclear overlap function in a given centrality class.

The $\langle T_{\mathrm{pPb}} \rangle_{\mathrm{i}}$ is estimated with the hybrid approach described in ref. [69] and is based on the assumption that the charged-particle multiplicity measured at mid-rapidity ($-1 < \eta_{\mathrm{cms}} < 0$) scales with the number of participant nucleons, N_{part}. The average nuclear overlap function is defined as $\langle T_{\mathrm{pPb}} \rangle_{\mathrm{i}} = \frac{\langle N_{\mathrm{coll}} \rangle_{\mathrm{i}}}{\sigma_{\mathrm{NN}}}$ where $\sigma_{\mathrm{NN}} = (67.6 \pm 0.6)$ mb is the interpolated inelastic nucleon–nucleon cross section at $\sqrt{s_{\mathrm{NN}}} = 5.02$ TeV [87] and $\langle N_{\mathrm{coll}} \rangle_{\mathrm{i}}$ is the average number of binary nucleon–nucleon collisions in a given centrality class. The latter is obtained as

$$\langle N_{\mathrm{coll}} \rangle_{\mathrm{i}} = \langle N_{\mathrm{part}} \rangle_{\mathrm{i}} - 1 = \langle N_{\mathrm{part}}^{\mathrm{MB}} \rangle \cdot \left(\frac{\langle \mathrm{d}N_{\mathrm{ch}}/\mathrm{d}\eta \rangle_{\mathrm{i}}}{\langle \mathrm{d}N_{\mathrm{ch}}/\mathrm{d}\eta \rangle^{\mathrm{MB}}} \right)_{-1 < \eta < 0} - 1 \,, \qquad (5.7)$$

where $\langle N_{\mathrm{part}}^{\mathrm{MB}} \rangle = 7.7$ [88] is the average number of participants in minimum bias collisions. The values of $\langle T_{\mathrm{pPb}} \rangle$ used for the analyses are reported in table 2 [88].

The average of prompt D^0, D^+, and D^{*+} meson Q_{pPb} was calculated as a function of p_{T} in the interval $1 < p_{\mathrm{T}} < 36$ GeV/c in 0–10%, 10–20%, 20–40%, 40–60%, and 60–100% centrality classes, and is shown in figure 10. The D-meson Q_{pPb} measurement shows a hint of suppression in the interval $1 < p_{\mathrm{T}} < 2$ GeV/c. The observed suppression is strongest in the most central collisions. This is qualitatively expected from a stronger shadowing at low Bjorken-x in central collisions. There is also a hint of enhancement at $2 < p_{\mathrm{T}} < 6$ GeV/c in the most central classes (0–40% centrality). The results are also compared with the charged-particle Q_{pPb} [69][1] in each centrality class. A similar trend is observed for prompt D mesons and charged particles in each centrality class.
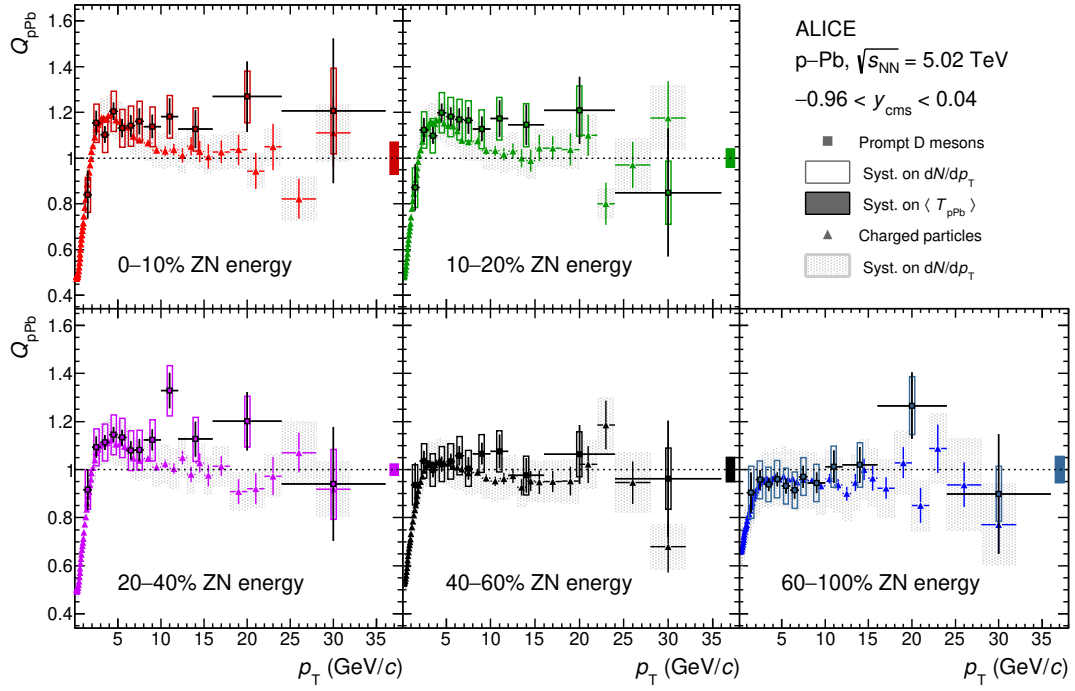
Figure 10. Nuclear modification factors of prompt D mesons as a function of p_T in 0–10%, 10–20%, 20–40%, 40–60%, and 60–100% centrality classes compared with those of charged particles [69]. The vertical bars represent the statistical uncertainties while the empty boxes and the shaded boxes represent the systematic uncertainties for the prompt D mesons and for the charged particles. The colour-filled boxes at $Q_{pPb} = 1$ represent the normalisation uncertainties on the $\langle T_{pPb} \rangle$ [88].
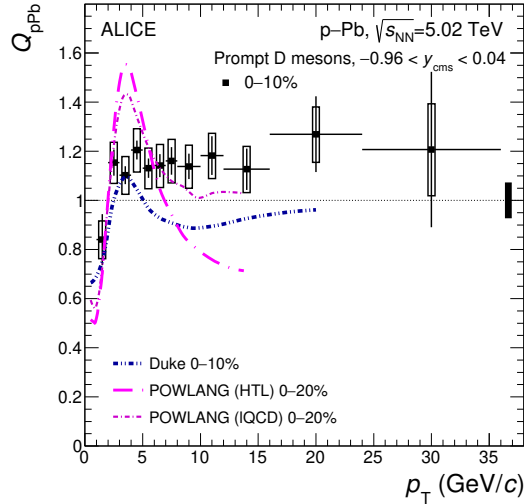
Figure 11. D-meson Q_{pPb} measured in the 0–10% centrality class compared with the predictions of the Duke [52] and POWLANG [53] transport models. The vertical bars and the empty boxes represent the statistical and systematic uncertainties. The colour-filled boxes at $Q_{pPb} = 1$ represent the normalisation uncertainties.

The D-meson Q_{pPb} in the 0–10% centrality class is compared with the predictions of the Duke [52] and POWLANG [53] transport models in figure 11. The POWLANG model predicts a pronounced bump in the nuclear modification factor at intermediate p_{T} ($3 < p_{\mathrm{T}} < 6\,\mathrm{GeV}/c$), which is not supported by the data, considering that the systematic uncertainties are mostly correlated among the p_{T} intervals of the measurement. At higher p_{T} ($p_{\mathrm{T}} > 7\,\mathrm{GeV}/c$), POWLANG simulations with the HTL transport coefficients and the Duke model predict a suppression of the D-meson yield which is not observed in the data.

The ratio of the D-meson yield in a given centrality class with respect to yield in the most peripheral centrality class (60–100%), defined as

$$Q_{\mathrm{CP}} = \frac{(\mathrm{d}^2 N^{\mathrm{prompt\,D}}/\mathrm{d}p_{\mathrm{T}}\mathrm{d}y)^{\mathrm{i}}_{\mathrm{p-Pb}}/\langle T_{\mathrm{pPb}}\rangle_{\mathrm{i}}}{(\mathrm{d}^2 N^{\mathrm{prompt\,D}}/\mathrm{d}p_{\mathrm{T}}\mathrm{d}y)^{60-100\%}_{\mathrm{p-Pb}}/\langle T_{\mathrm{pPb}}\rangle_{60-100\%}}, \tag{5.8}$$

was also calculated. The Q_{CP} observable is independent of the pp cross section and uses the yields in peripheral p–Pb collisions as a reference. Since the contributions from the track reconstruction, selection and PID efficiency cancel out in the ratio, the Q_{CP} has reduced systematic uncertainties with respect to the Q_{pPb} ratio. The systematic uncertainties on the yield extraction were estimated by applying the fit variation procedure described in section 4 directly on the signal yield ratio obtained from the invariant-mass distributions of the two centrality classes. To estimate the feed-down correction uncertainty, the contributions from the hypothesis on the nuclear modification factor of D mesons from B-hadron decays were considered as uncorrelated in each centrality class and were added in quadrature.

In figure 12, the average D-meson Q_{CP} is shown for different centrality classes: 0–10%, 10–20%, 20–40% and 40–60%. The results are superimposed to those obtained for charged particles in the same centrality classes [69]. A similar trend is observed for both measurements: when the results from the most central classes are used as the numerator, the Q_{CP} increases in the interval 1–5 GeV/c, reaching values of about 1.3 and then shows a decreasing trend with increasing p_{T}. A $Q_{\mathrm{CP}} > 1$ with a significance of 3σ is observed in the range $3 < p_{\mathrm{T}} < 7\,\mathrm{GeV}/c$ when the 20–40% centrality class is used as numerator. In this case, the normalisation uncertainty is smaller than the one of more central collisions due to the smaller separation between the centrality classes used in the calculation of Q_{CP}. When the 0–10% and 10–20% centrality classes are used as numerators, a $Q_{\mathrm{CP}} > 1$ is observed in the same p_{T} interval, with a significance of 1.5σ and 2σ due to the larger $\langle T_{\mathrm{pPb}}\rangle$ uncertainties. A milder p_{T} dependence is observed when the yields from more peripheral collisions are used as the numerator. A possible radial flow arising from a hydrodynamic evolution could modify the hadronisation dynamics of heavy quarks and potentially be the cause of the enhancement at intermediate p_{T}.

5.4 D-meson ratios

The ratios of the p_{T}-differential cross sections of D^0, D^+, D^{*+}, and $\mathrm{D}_{\mathrm{s}}^+$ mesons in the minimum bias sample are reported in figure 13. In the evaluation of the systematic uncertainties of the ratios, the contributions of the yield extraction and selection efficiency

---

[1]The $\langle T_{\mathrm{pPb}}\rangle$ values used to compute the charged-particles Q_{pPb} were updated with respect to [69] according to the values in [88].
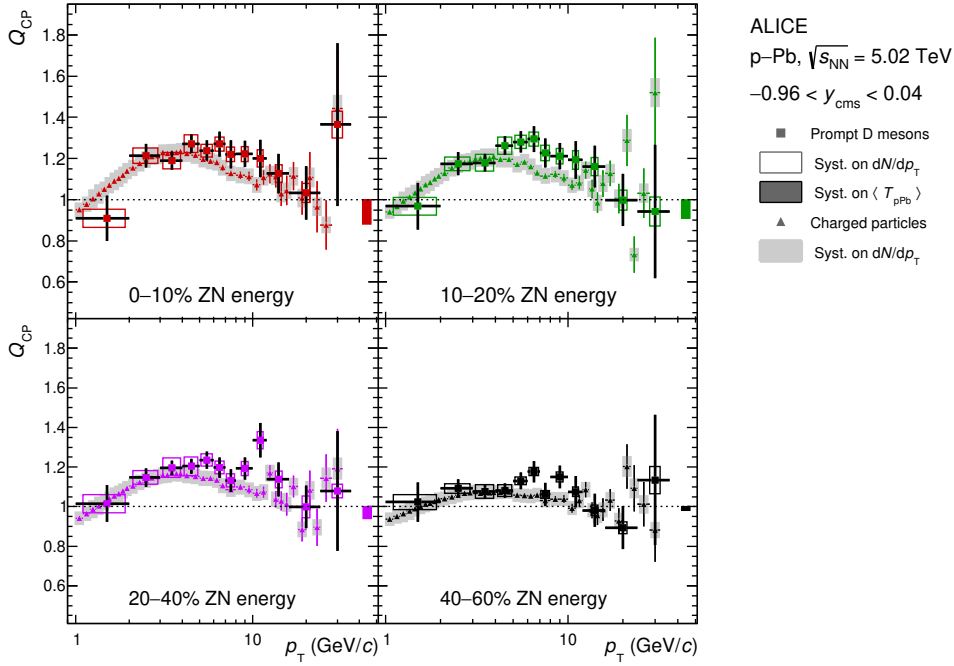
Figure 12. Average D-meson and charged-particles [69] Q_{CP} using the yields measured in 0–10%, 10–20%, 20–40%, and 40–60% as numerators and the yield in 60–100% as the denominator. The vertical bars and the empty boxes represent the statistical and systematic uncertainties. The colour-filled boxes at $Q_{\mathrm{CP}} = 1$ represent the normalisation uncertainties on the $\langle T_{\mathrm{pPb}} \rangle$.

were considered as uncorrelated, while those of the feed-down from beauty-hadron decays and the tracking efficiency were treated as fully correlated among the different D-meson species. The measurements are compared to the ratios of D-meson cross sections in pp collisions at $\sqrt{s} = 5$ TeV [70]. The relative abundances of the four species are unmodified in p–Pb with respect to pp collisions within statistical and systematic uncertainties.

The ratios of the $\mathrm{D_s^+/D^+}$-meson yields were also studied in different p_{T} intervals as a function the multiplicity of charged particles produced in the collision. The charged-particle multiplicity, N_{ch}, was estimated at mid-rapidity by measuring the number of tracklets, $N_{\mathrm{tracklets}}$ as in refs. [72, 89]. The $\mathrm{D_s^+/D^+}$ ratios were extracted in three multiplicity classes defined as 1–40, 40–70, 70–200 tracklets. A tracklet is defined as a track segment that joins the reconstructed primary vertex with a pair of space points on the two SPD layers within the pseudorapidity range $|\eta| < 1.0$. The measured $N_{\mathrm{tracklets}}$ distribution is affected by the position of the interaction vertex along the beam axis and by the evolution of the detector conditions. The former is due to the collision system asymmetry and the limited SPD rapidity coverage, while the latter is a consequence of a variation in active SPD channels over time. To account for these effects, the $N_{\mathrm{tracklets}}$ distributions were corrected offline on an event-by-event basis. The correlation between the measured $N_{\mathrm{tracklets}}$ and N_{ch}, equivalent to the number of generated "physical primaries", was obtained from a Monte Carlo simulation and parametrised with a linear function. Here, physical primaries are defined as prompt particles produced in the collision, along with their decay products, but
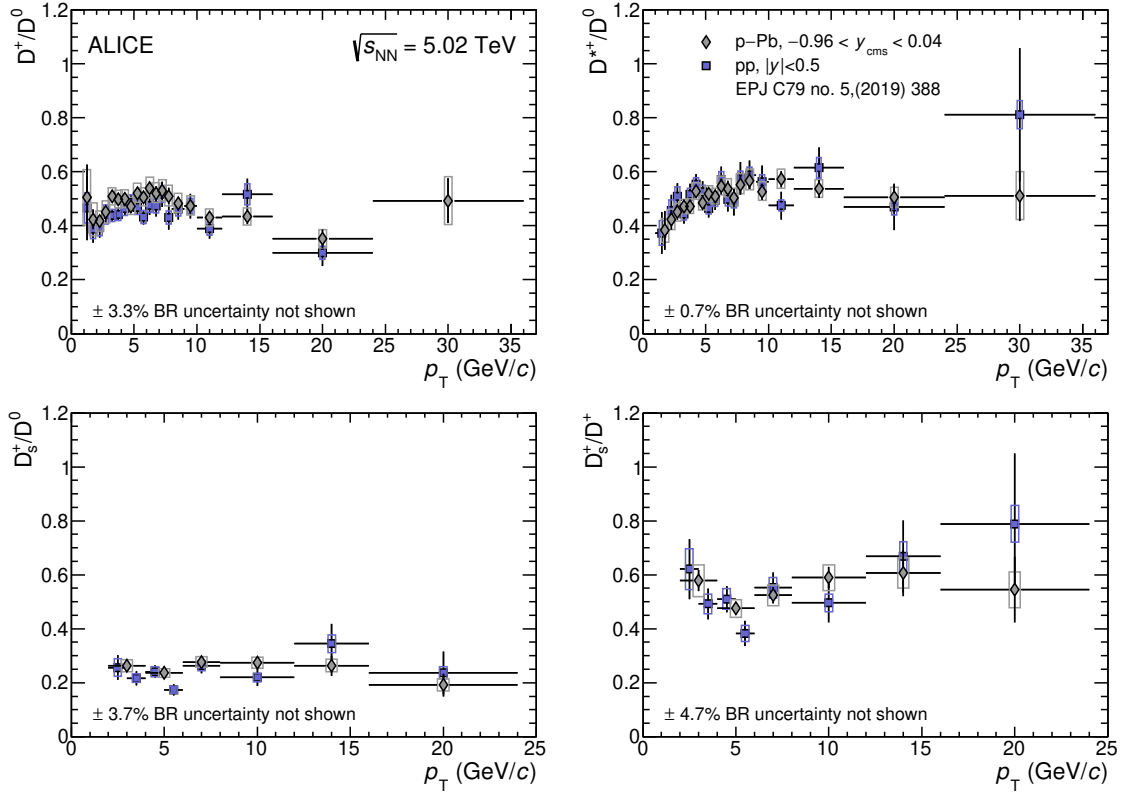
Figure 13. Ratios of prompt D-meson production cross sections as a function of p_T in p–Pb collisions at $\sqrt{s_{NN}} = 5.02$ TeV. The results are compared with those of pp collisions at the same centre-of-mass energy [70]. The vertical bars and the empty boxes represent the statistical and systematic uncertainties.

excluding those from weak decays of strange particles [78]. The systematic uncertainty on the conversion from $N_{\text{tracklets}}$ to N_{ch} was calculated using different Monte Carlo generators and using different parameterisations of the correlation. The total systematic uncertainty varies from 2% in the highest multiplicity class to 7% in the lowest multiplicity class.

The ratios of the D_s^+/D^+-meson yields are shown in figure 14 as a function of the number of primary charged particles per unity of pseudorapidity $(dN_{\text{ch}}/d\eta|_{|\eta|<0.5})$ in five p_T intervals ranging from 2 to 16 GeV/c. As a comparison, the measured ratios in pp collisions [70] and in Pb–Pb collisions [90] at $\sqrt{s_{NN}} = 5.02$ TeV are also shown in the figure. Within uncertainties, there is no indication of a modification of the D_s^+/D^+-yield ratios in pp and p–Pb collisions, up to the highest multiplicities that could be studied with the current p–Pb sample, which are similar to those of peripheral Pb–Pb collisions (60–80% centrality class). A hint of an enhancement of the D_s^+/D^+-yield ratios in Pb–Pb collisions in $4 < p_T < 8$ GeV/c is observed, as already shown in [90]. The larger data sample of Pb–Pb collisions collected by ALICE in 2018 will provide a more precise measurement.
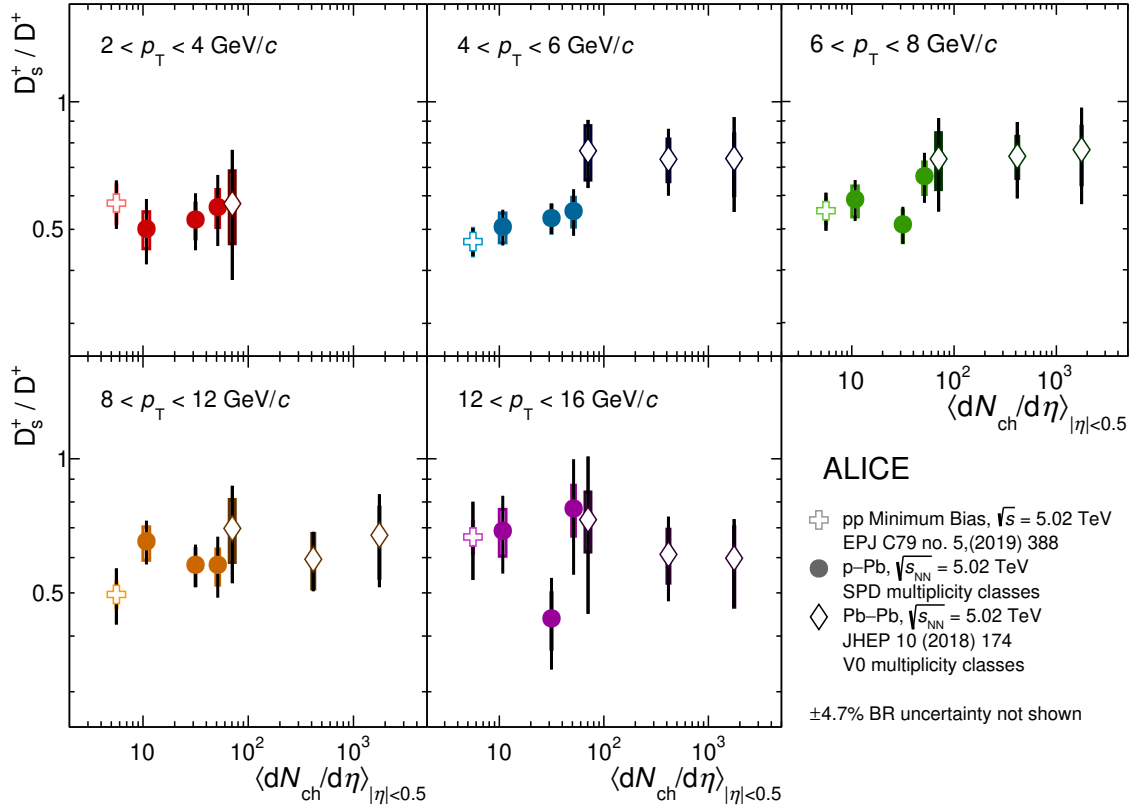
Figure 14. D_s^+/D^+-meson yield ratios, as a function of primary charged particles per unity of pseudorapidity in pp [70], p–Pb, and Pb–Pb [90] collisions at $\sqrt{s_{NN}} = 5.02$ TeV in five different p_T intervals from 2 to 16 GeV/c.

6 Summary

The production cross sections of the prompt charmed mesons (D^0, D^+, D^{*+}, and D_s^+) in p–Pb collisions at a centre-of-mass energy per nucleon pair of $\sqrt{s_{NN}} = 5.02$ TeV were measured as a function of p_T in the rapidity interval $-0.96 < y_{cms} < 0.04$ with luminosity of $L_{int} = 292 \pm 11$ μb^{-1}. The p_T-differential production cross sections were reported in the transverse momentum range $0 < p_T < 36$ GeV/c for D^0 mesons, $1 < p_T < 36$ GeV/c for D^+ mesons, $1.5 < p_T < 36$ GeV/c for D^{*+} mesons, and $2 < p_T < 24$ GeV/c for D_s^+ mesons. The larger sample used for this analysis, with respect to that collected in 2013, allowed for a significant reduction, by a factor 1.5–2, of the statistical and systematic uncertainties, along with an extension of the p_T reach.

The p_T-differential nuclear modification factor R_{pPb} of D mesons, calculated by using the pp reference measured at the same centre-of-mass energy, was found to be compatible with unity for $0 < p_T < 36$ GeV/c. The R_{pPb} results are described within uncertainties by theoretical calculations that include initial-state effects. The R_{pPb} is also compared with parton-transport model based calculations that assume the formation of a deconfined QCD medium in p–Pb collisions. The trend predicted by these models is not supported by

the data. The strong enhancement at $p_T \sim 3$–$4\,\mathrm{GeV}/c$ observed in the calculations is not consistent with the measured R_{pPb}, and a suppression larger than 10% for $p_T > 8\,\mathrm{GeV}/c$ is excluded by the data at 98% confidence level.

The centrality dependence of the D-meson yields was also studied in different centrality classes, from most central to peripheral collisions, in the interval $1 < p_T < 36\,\mathrm{GeV}/c$. The average Q_{pPb} of prompt D^0, D^+, and D^{*+} mesons is consistent with unity within the uncertainties for $p_T > 2\,\mathrm{GeV}/c$. The measurements show a hint of suppression in $1 < p_T < 2\,\mathrm{GeV}/c$ stronger in the most central collisions with respect to the peripheral ones, as qualitatively expected from a stronger shadowing at low Bjorken-x in central collisions [91, 92]. There is also a hint of enhancement in the intermediate p_T region in the most central collision classes (0–40% centrality). The same trend is observed for the charged-particles Q_{pPb}. The average D-meson Q_{CP} has been computed. For the most central collision classes, the Q_{CP} increases in the p_T interval 1–$5\,\mathrm{GeV}/c$, reaching values of about 1.3. Above a p_T of $5\,\mathrm{GeV}/c$ the distribution tends to decrease with increasing p_T. A milder p_T dependence is observed for more peripheral collisions. A similar trend is observed for both charmed mesons and charged particles in all the centrality classes considered. A possible radial flow arising from hydrodynamic evolution could modify the hadronisation dynamics of heavy quarks and give rise to the enhancement measured in the intermediate p_T interval [52, 53].

The ratios of the p_T-differential cross sections of D^0, D^+, D^{*+}, and D_s^+ mesons were evaluated and compared to those measured in pp collisions at $\sqrt{s} = 5.02$ TeV. The relative abundances of the four species are unmodified in p–Pb collisions with respect to pp collisions, within the uncertainties. The ratios of D_s^+/D^+-meson yields, as a function of the number of primary charged particles per unit of pseudorapidity, show no evidence of modifications in pp and p–Pb collisions, within the uncertainties.

A   Additional figures

Figure 15 presents the Q_{pPb} results for D^0, D^+, and D^{*+} as a function of p_T for the 0–10% and 60–100% centrality classes. Figure 16 shows the Q_{CP} for the three non-strange D mesons, obtained using 0–10% as central class and 60–100% as peripheral class. The results are compatible within uncertainties between the three D–meson species.
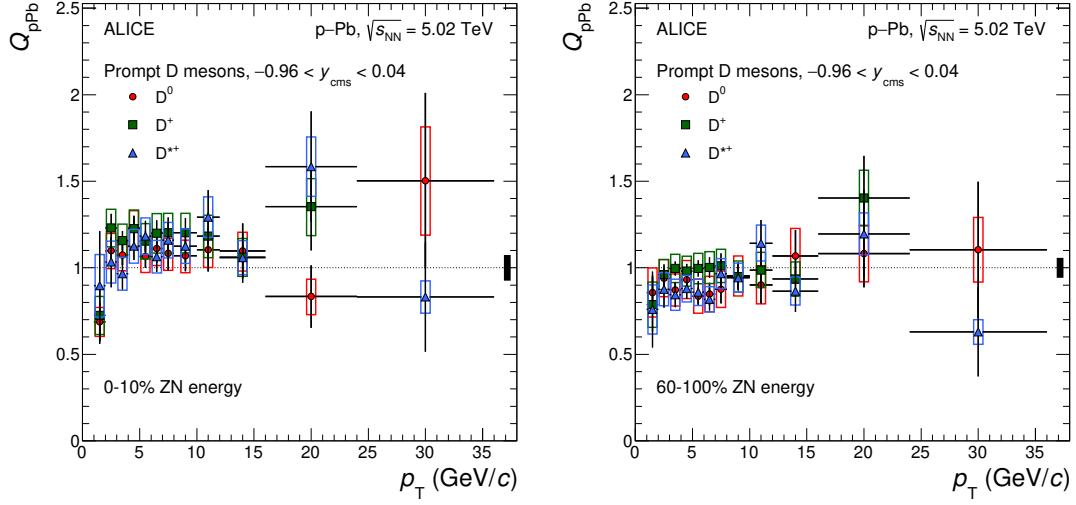
Figure 15. D^0, D^+, and D^{*+} meson nuclear modification factors as a function of p_T in the 0–10% (left) and 60–100% (right) centrality classes. The vertical bars and the empty boxes represent the statistical and systematic uncertainties. The colour-filled boxes at $Q_{pPb} = 1$ represent the normalisation uncertainties.
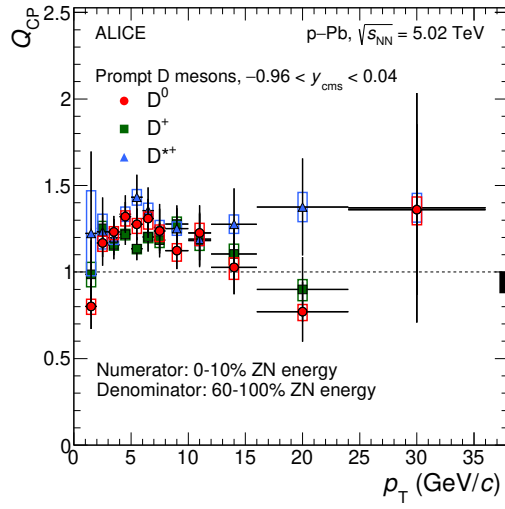
Figure 16. D^0, D^+, and D^{*+} meson Q_{CP}, obtained using 0–10% as the central class and 60–100% as the peripheral class. The vertical bars and the empty boxes represent the statistical and systematic uncertainties, respectively. The colour-filled boxes at $Q_{CP}= 1$ represent the normalisation uncertainties.

Acknowledgments

References

[1] M. Cacciari, M. Greco and P. Nason, *The p_T spectrum in heavy flavor hadroproduction*, *JHEP* **05** (1998) 007 [hep-ph/9803400] [INSPIRE].

[2] M. Cacciari, S. Frixione, N. Houdeau, M.L. Mangano, P. Nason and G. Ridolfi, *Theoretical predictions for charm and bottom production at the LHC*, *JHEP* **10** (2012) 137 [arXiv:1205.6344] [INSPIRE].

[3] B.A. Kniehl, G. Kramer, I. Schienbein and H. Spiesberger, *Inclusive $D^{*\pm}$ production in $p\bar{p}$ collisions with massive charm quarks*, *Phys. Rev.* **D 71** (2005) 014018 [hep-ph/0410289] [INSPIRE].

[4] B.A. Kniehl, G. Kramer, I. Schienbein and H. Spiesberger, *Collinear subtractions in hadroproduction of heavy quarks*, *Eur. Phys. J.* **C 41** (2005) 199 [hep-ph/0502194] [INSPIRE].

[5] B.A. Kniehl, G. Kramer, I. Schienbein and H. Spiesberger, *Inclusive Charmed-Meson Production at the CERN LHC*, *Eur. Phys. J.* **C 72** (2012) 2082 [arXiv:1202.0439] [INSPIRE].

[6] I. Helenius and H. Paukkunen, *Revisiting the D-meson hadroproduction in general-mass variable flavour number scheme*, *JHEP* **05** (2018) 196 [arXiv:1804.03557] [INSPIRE].

[7] A. Andronic et al., *Heavy-flavour and quarkonium production in the LHC era: from proton-proton to heavy-ion collisions*, *Eur. Phys. J.* **C 76** (2016) 107 [arXiv:1506.03981] [INSPIRE].

[8] F. Prino and R. Rapp, *Open Heavy Flavor in QCD Matter and in Nuclear Collisions*, *J. Phys.* **G 43** (2016) 093002 [arXiv:1603.00529] [INSPIRE].

[9] M. Arneodo, *Nuclear effects in structure functions*, *Phys. Rept.* **240** (1994) 301 [ɪɴSPIRE].

[10] S. Malace, D. Gaskell, D.W. Higinbotham and I. Cloet, *The Challenge of the EMC Effect: existing data and future directions*, *Int. J. Mod. Phys.* **E 23** (2014) 1430013 [arXiv:1405.1270] [ɪɴSPIRE].

[11] K.J. Eskola, H. Paukkunen and C.A. Salgado, *EPS09: A New Generation of NLO and LO Nuclear Parton Distribution Functions*, *JHEP* **04** (2009) 065 [arXiv:0902.4154] [ɪɴSPIRE].

[12] M. Hirai, S. Kumano and T.H. Nagai, *Determination of nuclear parton distribution functions and their uncertainties in next-to-leading order*, *Phys. Rev.* **C 76** (2007) 065207 [arXiv:0709.3038] [ɪɴSPIRE].

[13] D. de Florian and R. Sassot, *Nuclear parton distributions at next-to-leading order*, *Phys. Rev.* **D 69** (2004) 074028 [hep-ph/0311227] [ɪɴSPIRE].

[14] K.J. Eskola, P. Paakkinen, H. Paukkunen and C.A. Salgado, *EPPS16: Nuclear parton distributions with LHC data*, *Eur. Phys. J.* **C 77** (2017) 163 [arXiv:1612.05741] [ɪɴSPIRE].

[15] A. Kusina, J.-P. Lansberg, I. Schienbein and H.-S. Shao, *Gluon Shadowing in Heavy-Flavor Production at the LHC*, *Phys. Rev. Lett.* **121** (2018) 052004 [arXiv:1712.07024] [ɪɴSPIRE].

[16] K.J. Eskola, I. Helenius, P. Paakkinen and H. Paukkunen, *A QCD analysis of LHCb D-meson data in p+Pb collisions*, arXiv:1906.02512 [ɪɴSPIRE].

[17] F. Gelis, E. Iancu, J. Jalilian-Marian and R. Venugopalan, *The Color Glass Condensate*, *Ann. Rev. Nucl. Part. Sci.* **60** (2010) 463 [arXiv:1002.0333] [ɪɴSPIRE].

[18] P. Tribedy and R. Venugopalan, *QCD saturation at the LHC: Comparisons of models to p+p and A+A data and predictions for p+Pb collisions*, *Phys. Lett.* **B 710** (2012) 125 [*Erratum ibid.* **B 718** (2013) 1154] [arXiv:1112.2445] [ɪɴSPIRE].

[19] J.L. Albacete, A. Dumitru, H. Fujii and Y. Nara, *CGC predictions for p + Pb collisions at the LHC*, *Nucl. Phys.* **A 897** (2013) 1 [arXiv:1209.2001] [ɪɴSPIRE].

[20] A.H. Rezaeian, *CGC predictions for p + A collisions at the LHC and signature of QCD saturation*, *Phys. Lett.* **B 718** (2013) 1058 [arXiv:1210.2385] [ɪɴSPIRE].

[21] H. Fujii and K. Watanabe, *Heavy quark pair production in high energy pA collisions: Open heavy flavors*, *Nucl. Phys.* **A 920** (2013) 78 [arXiv:1308.1258] [ɪɴSPIRE].

[22] I. Vitev, *Non-Abelian energy loss in cold nuclear matter*, *Phys. Rev.* **C 75** (2007) 064906 [hep-ph/0703002] [ɪɴSPIRE].

[23] M. Lev and B. Petersson, *Nuclear Effects at Large Transverse Momentum in a QCD Parton Model*, *Z. Phys.* **C 21** (1983) 155 [ɪɴSPIRE].

[24] X.-N. Wang, *Systematic study of high p_T hadron spectra in pp, pA and AA collisions from SPS to RHIC energies*, *Phys. Rev.* **C 61** (2000) 064910 [nucl-th/9812021] [ɪɴSPIRE].

[25] B.Z. Kopeliovich, J. Nemchik, A. Schafer and A.V. Tarasov, *Cronin effect in hadron production off nuclei*, *Phys. Rev. Lett.* **88** (2002) 232303 [hep-ph/0201010] [ɪɴSPIRE].

[26] CMS collaboration, *Observation of Long-Range Near-Side Angular Correlations in Proton-Lead Collisions at the LHC*, *Phys. Lett.* **B 718** (2013) 795 [arXiv:1210.5482] [ɪɴSPIRE].

[27] ALICE collaboration, *Long-range angular correlations on the near and away side in p-Pb collisions at $\sqrt{s_{NN}} = 5.02$ TeV*, *Phys. Lett.* **B 719** (2013) 29 [arXiv:1212.2001] [ɪɴSPIRE].

[28] ALICE collaboration, *Long-range angular correlations of π, K and p in p-Pb collisions at* $\sqrt{s_{\mathrm{NN}}} = 5.02\,TeV$, *Phys. Lett.* **B 726** (2013) 164 [arXiv:1307.3237] [INSPIRE].

[29] ATLAS collaboration, *Observation of Associated Near-Side and Away-Side Long-Range Correlations in* $\sqrt{s_{NN}} = 5.02\,TeV$ *Proton-Lead Collisions with the ATLAS Detector*, *Phys. Rev. Lett.* **110** (2013) 182302 [arXiv:1212.5198] [INSPIRE].

[30] ALICE collaboration, *Forward-central two-particle correlations in p-Pb collisions at* $\sqrt{s_{\mathrm{NN}}} = 5.02\,TeV$, *Phys. Lett.* **B 753** (2016) 126 [arXiv:1506.08032] [INSPIRE].

[31] LHCb collaboration, *Measurements of long-range near-side angular correlations in* $\sqrt{s_{NN}} = 5\,TeV$ *proton-lead collisions in the forward region*, *Phys. Lett.* **B 762** (2016) 473 [arXiv:1512.00439] [INSPIRE].

[32] CMS collaboration, *Evidence for Collective Multiparticle Correlations in p-Pb Collisions*, *Phys. Rev. Lett.* **115** (2015) 012301 [arXiv:1502.05382] [INSPIRE].

[33] ATLAS collaboration, *Measurement of long-range multiparticle azimuthal correlations with the subevent cumulant method in pp and* $p + Pb$ *collisions with the ATLAS detector at the CERN Large Hadron Collider*, *Phys. Rev.* **C 97** (2018) 024904 [arXiv:1708.03559] [INSPIRE].

[34] ALICE collaboration, *Multiplicity Dependence of Pion, Kaon, Proton and Lambda Production in p-Pb Collisions at* $\sqrt{s_{NN}} = 5.02\,TeV$, *Phys. Lett.* **B 728** (2014) 25 [arXiv:1307.6796] [INSPIRE].

[35] CMS collaboration, *Study of the Production of Charged Pions, Kaons and Protons in pPb Collisions at* $\sqrt{s_{NN}} = 5.02\,TeV$, *Eur. Phys. J.* **C 74** (2014) 2847 [arXiv:1307.3442] [INSPIRE].

[36] ALICE collaboration, *Suppression of* $\psi(2S)$ *production in p-Pb collisions at* $\sqrt{s_{\mathrm{NN}}} = 5.02\,TeV$, *JHEP* **12** (2014) 073 [arXiv:1405.3796] [INSPIRE].

[37] LHCb collaboration, *Study of* $\psi(2S)$ *production and cold nuclear matter effects in pPb collisions at* $\sqrt{s_{NN}} = 5\,TeV$, *JHEP* **03** (2016) 133 [arXiv:1601.07878] [INSPIRE].

[38] ALICE collaboration, *Centrality dependence of* $\psi(2S)$ *suppression in p-Pb collisions at* $\sqrt{s_{\mathrm{NN}}} = 5.02\,TeV$, *JHEP* **06** (2016) 050 [arXiv:1603.02816] [INSPIRE].

[39] WUPPERTAL-BUDAPEST collaboration, *Is there still any* T_c *mystery in lattice QCD? Results with physical masses in the continuum limit III*, *JHEP* **09** (2010) 073 [arXiv:1005.3508] [INSPIRE].

[40] A. Bazavov et al., *The chiral and deconfinement aspects of the QCD transition*, *Phys. Rev.* **D 85** (2012) 054503 [arXiv:1111.1710] [INSPIRE].

[41] A. Jaiswal and V. Roy, *Relativistic hydrodynamics in heavy-ion collisions: general aspects and recent developments*, *Adv. High Energy Phys.* **2016** (2016) 9623034 [arXiv:1605.08694] [INSPIRE].

[42] W. Busza, K. Rajagopal and W. van der Schee, *Heavy Ion Collisions: The Big Picture and the Big Questions*, *Ann. Rev. Nucl. Part. Sci.* **68** (2018) 339 [arXiv:1802.04801] [INSPIRE].

[43] J.L. Nagle and W.A. Zajc, *Small System Collectivity in Relativistic Hadronic and Nuclear Collisions*, *Ann. Rev. Nucl. Part. Sci.* **68** (2018) 211 [arXiv:1801.03477] [INSPIRE].

[44] P. Bozek and W. Broniowski, *Correlations from hydrodynamic flow in p-Pb collisions*, *Phys. Lett.* **B 718** (2013) 1557 [arXiv:1211.0845] [INSPIRE].

[45] P. Bozek and W. Broniowski, *Collective dynamics in high-energy proton-nucleus collisions*, *Phys. Rev.* **C 88** (2013) 014903 [arXiv:1304.3044] [ɪɴSPIRE].

[46] R.D. Weller and P. Romatschke, *One fluid to rule them all: viscous hydrodynamic description of event-by-event central p+p, p+Pb and Pb+Pb collisions at $\sqrt{s} = 5.02$ TeV*, *Phys. Lett.* **B 774** (2017) 351 [arXiv:1701.07145] [ɪɴSPIRE].

[47] K. Dusling and R. Venugopalan, *Evidence for BFKL and saturation dynamics from dihadron spectra at the LHC*, *Phys. Rev.* **D 87** (2013) 051502 [arXiv:1210.3890] [ɪɴSPIRE].

[48] K. Dusling, W. Li and B. Schenke, *Novel collective phenomena in high-energy proton-proton and proton-nucleus collisions*, *Int. J. Mod. Phys.* **E 25** (2016) 1630002 [arXiv:1509.07939] [ɪɴSPIRE].

[49] L. He, T. Edmonds, Z.-W. Lin, F. Liu, D. Molnar and F. Wang, *Anisotropic parton escape is the dominant source of azimuthal anisotropy in transport models*, *Phys. Lett.* **B 753** (2016) 506 [arXiv:1502.05572] [ɪɴSPIRE].

[50] C. Bierlich, G. Gustafson, L. Lönnblad and A. Tarasov, *Effects of Overlapping Strings in pp Collisions*, *JHEP* **03** (2015) 148 [arXiv:1412.6259] [ɪɴSPIRE].

[51] C. Bierlich, G. Gustafson and L. Lönnblad, *Collectivity without plasma in hadronic collisions*, *Phys. Lett.* **B 779** (2018) 58 [arXiv:1710.09725] [ɪɴSPIRE].

[52] Y. Xu et al., *Heavy-flavor dynamics in relativistic p-Pb collisions at $\sqrt{S_{NN}} = 5.02$ TeV*, *Nucl. Part. Phys. Proc.* **276–278** (2016) 225 [arXiv:1510.07520] [ɪɴSPIRE].

[53] A. Beraudo, A. De Pace, M. Monteno, M. Nardi and F. Prino, *Heavy-flavour production in high-energy d-Au and p-Pb collisions*, *JHEP* **03** (2016) 123 [arXiv:1512.05186] [ɪɴSPIRE].

[54] ALICE collaboration, *Search for collectivity with azimuthal J/ψ-hadron correlations in high multiplicity p-Pb collisions at $\sqrt{s_{\mathrm{NN}}} = 5.02$ and 8.16 TeV*, *Phys. Lett.* **B 780** (2018) 7 [arXiv:1709.06807] [ɪɴSPIRE].

[55] CMS collaboration, *Elliptic flow of charm and strange hadrons in high-multiplicity pPb collisions at $\sqrt{s_{\mathrm{NN}}} = 8.16$ TeV*, *Phys. Rev. Lett.* **121** (2018) 082301 [arXiv:1804.09767] [ɪɴSPIRE].

[56] ALICE collaboration, *Azimuthal Anisotropy of Heavy-Flavor Decay Electrons in p-Pb Collisions at $\sqrt{s_{\mathrm{NN}}} = 5.02$ TeV*, *Phys. Rev. Lett.* **122** (2019) 072301 [arXiv:1805.04367] [ɪɴSPIRE].

[57] V. Greco, C.M. Ko and P. Levai, *Parton coalescence at RHIC*, *Phys. Rev.* **C 68** (2003) 034904 [nucl-th/0305024] [ɪɴSPIRE].

[58] V. Greco, C.M. Ko and R. Rapp, *Quark coalescence for charmed mesons in ultrarelativistic heavy ion collisions*, *Phys. Lett.* **B 595** (2004) 202 [nucl-th/0312100] [ɪɴSPIRE].

[59] A. Andronic, P. Braun-Munzinger, K. Redlich and J. Stachel, *Charmonium and open charm production in nuclear collisions at SPS/FAIR energies and the possible influence of a hot hadronic medium*, *Phys. Lett.* **B 659** (2008) 149 [arXiv:0708.1488] [ɪɴSPIRE].

[60] M. He, R.J. Fries and R. Rapp, **D_s**-*Meson as Quantitative Probe of Diffusion and Hadronization in Nuclear Collisions*, *Phys. Rev. Lett.* **110** (2013) 112301 [arXiv:1204.4442] [ɪɴSPIRE].

[61] ALICE collaboration, *Multi-strange baryon production in p-Pb collisions at $\sqrt{s_{\mathbf{NN}}} = 5.02$ TeV*, *Phys. Lett.* **B 758** (2016) 389 [arXiv:1512.07227] [ɪɴSPIRE].

[62] ALICE collaboration, *Enhanced production of multi-strange hadrons in high-multiplicity proton-proton collisions*, *Nature Phys.* **13** (2017) 535 [arXiv:1606.07424] [INSPIRE].

[63] ALICE collaboration, *Measurement of prompt D-meson production in p − Pb collisions at* $\sqrt{s_{NN}} = 5.02$ *TeV*, *Phys. Rev. Lett.* **113** (2014) 232301 [arXiv:1405.3452] [INSPIRE].

[64] ALICE collaboration, *Measurement of D-meson production versus multiplicity in p-Pb collisions at* $\sqrt{s_{NN}} = 5.02$ *TeV*, *JHEP* **08** (2016) 078 [arXiv:1602.07240] [INSPIRE].

[65] ALICE collaboration, *D-meson production in p-Pb collisions at* $\sqrt{s_{NN}} = 5.02$ *TeV and in pp collisions at* $\sqrt{s} = 7$ *TeV*, *Phys. Rev.* **C 94** (2016) 054908 [arXiv:1605.07569] [INSPIRE].

[66] ALICE collaboration, *The ALICE experiment at the CERN LHC*, 2008 *JINST* **3** S08002 [INSPIRE].

[67] ALICE collaboration, *Performance of the ALICE Experiment at the CERN LHC*, *Int. J. Mod. Phys.* **A 29** (2014) 1430044 [arXiv:1402.4476] [INSPIRE].

[68] ALICE collaboration, *Measurement of visible cross sections in proton-lead collisions at* $\sqrt{s_{NN}} = 5.02$ *TeV in van der Meer scans with the ALICE detector*, 2014 *JINST* **9** P11003 [arXiv:1405.1849] [INSPIRE].

[69] ALICE collaboration, *Centrality dependence of particle production in p-Pb collisions at* $\sqrt{s_{NN}} = 5.02$ *TeV*, *Phys. Rev.* **C 91** (2015) 064905 [arXiv:1412.6828] [INSPIRE].

[70] ALICE collaboration, *Measurement of* D^0, D^+, D^{*+} *and* D_s^+ *production in pp collisions at* $\sqrt{s} = 5.02$ *TeV with ALICE*, *Eur. Phys. J.* **C 79** (2019) 388 [arXiv:1901.07979] [INSPIRE].

[71] PARTICLE DATA GROUP collaboration, *Review of Particle Physics*, *Phys. Rev.* **D 98** (2018) 030001 [INSPIRE].

[72] ALICE collaboration, *Measurement of charm and beauty production at central rapidity versus charged-particle multiplicity in proton-proton collisions at* $\sqrt{s} = 7$ *TeV*, *JHEP* **09** (2015) 148 [arXiv:1505.00664] [INSPIRE].

[73] T. Sjöstrand, S. Mrenna and P.Z. Skands, *PYTHIA 6.4 Physics and Manual*, *JHEP* **05** (2006) 026 [hep-ph/0603175] [INSPIRE].

[74] X.-N. Wang and M. Gyulassy, *HIJING: A Monte Carlo model for multiple jet production in pp, pA and AA collisions*, *Phys. Rev.* **D 44** (1991) 3501 [INSPIRE].

[75] ALICE collaboration, *Measurement of D-meson production at mid-rapidity in pp collisions at* $\sqrt{s} = 7$ *TeV*, *Eur. Phys. J.* **C 77** (2017) 550 [arXiv:1702.00766] [INSPIRE].

[76] A. Ryd et al., *EvtGen: A Monte Carlo Generator for B-Physics*, EVTGEN-V00-11-07 [INSPIRE].

[77] CMS collaboration, *Study of B Meson Production in p+Pb Collisions at* $\sqrt{s_{NN}} = 5.02$ *TeV Using Exclusive Hadronic Decays*, *Phys. Rev. Lett.* **116** (2016) 032301 [arXiv:1508.06678] [INSPIRE].

[78] ALICE collaboration, *The ALICE definition of primary particles*, ALICE-PUBLIC-2017-005 (2017).

[79] L. Gladilin, *Fragmentation fractions of c and b quarks into charmed hadrons at LEP*, *Eur. Phys. J.* **C 75** (2015) 19 [arXiv:1404.3888] [INSPIRE].

[80] ALICE collaboration, Λ_c^+ *production in pp collisions at* $\sqrt{s} = 7$ *TeV and in p-Pb collisions at* $\sqrt{s_{NN}} = 5.02$ *TeV*, *JHEP* **04** (2018) 108 [arXiv:1712.09581] [INSPIRE].

[81] LHCb collaboration, *Prompt Λ_c^+ production in pPb collisions at $\sqrt{s_{NN}} = 5.02$ TeV*, *JHEP* **02** (2019) 102 [arXiv:1809.01404] [INSPIRE].

[82] H. Fujii and K. Watanabe, *Nuclear modification of forward D production in pPb collisions at the LHC*, arXiv:1706.06728 [INSPIRE].

[83] J. Pumplin, D.R. Stump, J. Huston, H.L. Lai, P.M. Nadolsky and W.K. Tung, *New generation of parton distributions with uncertainties from global QCD analysis*, *JHEP* **07** (2002) 012 [hep-ph/0201195] [INSPIRE].

[84] LHCb collaboration, *Study of prompt D^0 meson production in pPb collisions at $\sqrt{s_{NN}} = 5$ TeV*, *JHEP* **10** (2017) 090 [arXiv:1707.02750] [INSPIRE].

[85] R. Sharma, I. Vitev and B.-W. Zhang, *Light-cone wave function approach to open heavy flavor dynamics in QCD matter*, *Phys. Rev.* **C 80** (2009) 054902 [arXiv:0904.0032] [INSPIRE].

[86] Z.-B. Kang, I. Vitev, E. Wang, H. Xing and C. Zhang, *Multiple scattering effects on heavy meson production in p+A collisions at backward rapidity*, *Phys. Lett.* **B 740** (2015) 23 [arXiv:1409.2494] [INSPIRE].

[87] C. Loizides, J. Kamin and D. d'Enterria, *Improved Monte Carlo Glauber predictions at present and future nuclear colliders*, *Phys. Rev.* **C 97** (2018) 054910 [arXiv:1710.07098] [INSPIRE].

[88] ALICE collaboration, *Centrality determination in heavy ion collisions*, ALICE-PUBLIC-2018-011 (2018).

[89] ALICE collaboration, *J/ψ Production as a Function of Charged Particle Multiplicity in pp Collisions at $\sqrt{s} = 7$ TeV*, *Phys. Lett.* **B 712** (2012) 165 [arXiv:1202.2816] [INSPIRE].

[90] ALICE collaboration, *Measurement of D^0, D^+, D^{*+} and D_s^+ production in Pb-Pb collisions at $\sqrt{s_{NN}} = 5.02$ TeV*, *JHEP* **10** (2018) 174 [arXiv:1804.09083] [INSPIRE].

[91] K.J. Eskola, *Shadowing effects on quark and gluon production in ultrarelativistic heavy ion collisions*, *Z. Phys.* **C 51** (1991) 633 [INSPIRE].

[92] I. Helenius, K.J. Eskola, H. Honkanen and C.A. Salgado, *Impact-Parameter Dependent Nuclear Parton Distribution Functions: EPS09s and EKS98s and Their Applications in Nuclear Hard Processes*, *JHEP* **07** (2012) 073 [arXiv:1205.5359] [INSPIRE].

The ALICE collaboration

S. Acharya[141], D. Adamová[93], S.P. Adhya[141], A. Adler[73], J. Adolfsson[79], M.M. Aggarwal[98],
G. Aglieri Rinella[34], M. Agnello[31], N. Agrawal[10,48,53], Z. Ahammed[141], S. Ahmad[17], S.U. Ahn[75],
A. Akindinov[90], M. Al-Turany[105], S.N. Alam[141], D.S.D. Albuquerque[122], D. Aleksandrov[86],
B. Alessandro[58], H.M. Alfanda[6], R. Alfaro Molina[71], B. Ali[17], Y. Ali[15], A. Alici[10,27,53],
A. Alkin[2], J. Alme[22], T. Alt[68], L. Altenkamper[22], I. Altsybeev[112], M.N. Anaam[6], C. Andrei[47],
D. Andreou[34], H.A. Andrews[109], A. Andronic[144], M. Angeletti[34], V. Anguelov[102], C. Anson[16],
T. Antičić[106], F. Antinori[56], P. Antonioli[53], R. Anwar[125], N. Apadula[78], L. Aphecetche[114],
H. Appelshäuser[68], S. Arcelli[27], R. Arnaldi[58], M. Arratia[78], I.C. Arsene[21], M. Arslandok[102],
A. Augustinus[34], R. Averbeck[105], S. Aziz[61], M.D. Azmi[17], A. Badalà[55], Y.W. Baek[40],
S. Bagnasco[58], X. Bai[105], R. Bailhache[68], R. Bala[99], A. Baldisseri[137], M. Ball[42], S. Balouza[103],
R.C. Baral[84], R. Barbera[28], L. Barioglio[26], G.G. Barnaföldi[145], L.S. Barnby[92], V. Barret[134],
P. Bartalini[6], K. Barth[34], E. Bartsch[68], F. Baruffaldi[29], N. Bastid[134], S. Basu[143], G. Batigne[114],
B. Batyunya[74], P.C. Batzing[21], D. Bauri[48], J.L. Bazo Alba[110], I.G. Bearden[87], C. Bedda[63],
N.K. Behera[60], I. Belikov[136], F. Bellini[34], R. Bellwied[125], V. Belyaev[91], G. Bencedi[145], S. Beole[26],
A. Bercuci[47], Y. Berdnikov[96], D. Berenyi[145], R.A. Bertens[130], D. Berzano[58], M.G. Besoiu[67],
L. Betev[34], A. Bhasin[99], I.R. Bhat[99], M.A. Bhat[3], H. Bhatt[48], B. Bhattacharjee[41], A. Bianchi[26],
L. Bianchi[26,125], N. Bianchi[51], J. Bielčík[37], J. Bielčíková[93], A. Bilandzic[103,117], G. Biro[145],
R. Biswas[3], S. Biswas[3], J.T. Blair[119], D. Blau[86], C. Blume[68], G. Boca[139], F. Bock[34,94],
A. Bogdanov[91], L. Boldizsár[145], A. Bolozdynya[91], M. Bombara[38], G. Bonomi[140], H. Borel[137],
A. Borissov[91,144], M. Borri[127], H. Bossi[146], E. Botta[26], L. Bratrud[68], P. Braun-Munzinger[105],
M. Bregant[121], T.A. Broker[68], M. Broz[37], E.J. Brucken[43], E. Bruna[58], G.E. Bruno[33,104],
M.D. Buckland[127], D. Budnikov[107], H. Buesching[68], S. Bufalino[31], O. Bugnon[114], P. Buhler[113],
P. Buncic[34], Z. Buthelezi[72], J.B. Butt[15], J.T. Buxton[95], S.A. Bysiak[118], D. Caffarri[88],
A. Caliva[105], E. Calvo Villar[110], R.S. Camacho[44], P. Camerini[25], A.A. Capon[113],
F. Carnesecchi[10], J. Castillo Castellanos[137], A.J. Castro[130], E.A.R. Casula[54], F. Catalano[31],
C. Ceballos Sanchez[52], P. Chakraborty[48], S. Chandra[141], B. Chang[126], W. Chang[6],
S. Chapeland[34], M. Chartier[127], S. Chattopadhyay[141], S. Chattopadhyay[108], A. Chauvin[24],
C. Cheshkov[135], B. Cheynis[135], V. Chibante Barroso[34], D.D. Chinellato[122], S. Cho[60],
P. Chochula[34], T. Chowdhury[134], P. Christakoglou[88], C.H. Christensen[87], P. Christiansen[79],
T. Chujo[133], C. Cicalo[54], L. Cifarelli[10,27], F. Cindolo[53], J. Cleymans[124], F. Colamaria[52],
D. Colella[52], A. Collu[78], M. Colocci[27], M. Concas[58, ii], G. Conesa Balbastre[77], Z. Conesa del
Valle[61], G. Contin[59,127], J.G. Contreras[37], T.M. Cormier[94], Y. Corrales Morales[26,58],
P. Cortese[32], M.R. Cosentino[123], F. Costa[34], S. Costanza[139], J. Crkovská[61], P. Crochet[134],
E. Cuautle[69], L. Cunqueiro[94], D. Dabrowski[142], T. Dahms[103,117], A. Dainese[56],
F.P.A. Damas[114,137], S. Dani[65], M.C. Danisch[102], A. Danu[67], D. Das[108], I. Das[108], P. Das[3],
S. Das[3], A. Dash[84], S. Dash[48], A. Dashi[103], S. De[49,84], A. De Caro[30], G. de Cataldo[52], C. de
Conti[121], J. de Cuveland[39], A. De Falco[24], D. De Gruttola[10], N. De Marco[58], S. De Pasquale[30],
R.D. De Souza[122], S. Deb[49], H.F. Degenhardt[121], K.R. Deja[142], A. Deloff[83], S. Delsanto[26,131],
P. Dhankher[48], D. Di Bari[33], A. Di Mauro[34], R.A. Diaz[8], T. Dietel[124], P. Dillenseger[68], Y. Ding[6],
R. Divià[34], Ø. Djuvsland[22], U. Dmitrieva[62], A. Dobrin[34,67], B. Dönigus[68], O. Dordic[21],
A.K. Dubey[141], A. Dubla[105], S. Dudi[98], M. Dukhishyam[84], P. Dupieux[134], R.J. Ehlers[146],
D. Elia[52], H. Engel[73], E. Epple[146], B. Erazmus[114], F. Erhardt[97], A. Erokhin[112], M.R. Ersdal[22],
B. Espagnon[61], G. Eulisse[34], J. Eum[18], D. Evans[109], S. Evdokimov[89], L. Fabbietti[103,117],
M. Faggin[29], J. Faivre[77], A. Fantoni[51], M. Fasel[94], P. Fecchio[31], A. Feliciello[58], G. Feofilov[112],
A. Fernández Téllez[44], A. Ferrero[137], A. Ferretti[26], A. Festanti[34], V.J.G. Feuillard[102], J. Figiel[118],
S. Filchagin[107], D. Finogeev[62], F.M. Fionda[22], G. Fiorenza[52], F. Flor[125], S. Foertsch[72], P. Foka[105],

S. Fokin[86], E. Fragiacomo[59], U. Frankenfeld[105], G.G. Fronze[26], U. Fuchs[34], C. Furget[77],
A. Furs[62], M. Fusco Girard[30], J.J. Gaardhøje[87], M. Gagliardi[26], A.M. Gago[110], A. Gal[136],
C.D. Galvan[120], P. Ganoti[82], C. Garabatos[105], E. Garcia-Solis[11], K. Garg[28], C. Gargiulo[34],
A. Garibli[85], K. Garner[144], P. Gasik[103,117], E.F. Gauger[119], M.B. Gay Ducati[70], M. Germain[114],
J. Ghosh[108], P. Ghosh[141], S.K. Ghosh[3], P. Gianotti[51], P. Giubellino[58,105], P. Giubilato[29],
P. Glässel[102], D.M. Goméz Coral[71], A. Gomez Ramirez[73], V. Gonzalez[105], P. González-Zamora[44],
S. Gorbunov[39], L. Görlich[118], S. Gotovac[35], V. Grabski[71], L.K. Graczykowski[142],
K.L. Graham[109], L. Greiner[78], A. Grelli[63], C. Grigoras[34], V. Grigoriev[91], A. Grigoryan[1],
S. Grigoryan[74], O.S. Groettvik[22], J.M. Gronefeld[105], F. Grosa[31], J.F. Grosse-Oetringhaus[34],
R. Grosso[105], R. Guernane[77], B. Guerzoni[27], M. Guittiere[114], K. Gulbrandsen[87], T. Gunji[132],
A. Gupta[99], R. Gupta[99], I.B. Guzman[44], R. Haake[34,146], M.K. Habib[105], C. Hadjidakis[61],
H. Hamagaki[80], G. Hamar[145], M. Hamid[6], R. Hannigan[119], M.R. Haque[63], A. Harlenderova[105],
J.W. Harris[146], A. Harton[11], J.A. Hasenbichler[34], H. Hassan[77], D. Hatzifotiadou[10,53], P. Hauer[42],
S. Hayashi[132], A.D.L.B. Hechavarria[144], S.T. Heckel[68], E. Hellbär[68], H. Helstrup[36],
A. Herghelegiu[47], E.G. Hernandez[44], G. Herrera Corral[9], F. Herrmann[144], K.F. Hetland[36],
T.E. Hilden[43], H. Hillemanns[34], C. Hills[127], B. Hippolyte[136], B. Hohlweger[103], D. Horak[37],
S. Hornung[105], R. Hosokawa[133], P. Hristov[34], C. Huang[61], C. Hughes[130], P. Huhn[68],
T.J. Humanic[95], H. Hushnud[108], L.A. Husova[144], N. Hussain[41], S.A. Hussain[15], T. Hussain[17],
D. Hutter[39], D.S. Hwang[19], J.P. Iddon[34,127], R. Ilkaev[107], M. Inaba[133], M. Ippolitov[86],
M.S. Islam[108], M. Ivanov[105], V. Ivanov[96], V. Izucheev[89], B. Jacak[78], N. Jacazio[27], P.M. Jacobs[78],
M.B. Jadhav[48], S. Jadlovska[116], J. Jadlovsky[116], S. Jaelani[63], C. Jahnke[121], M.J. Jakubowska[142],
M.A. Janik[142], M. Jercic[97], O. Jevons[109], R.T. Jimenez Bustamante[105], M. Jin[125], F. Jonas[94,144],
P.G. Jones[109], A. Jusko[109], P. Kalinak[64], A. Kalweit[34], J.H. Kang[147], V. Kaplin[91], S. Kar[6],
A. Karasu Uysal[76], O. Karavichev[62], T. Karavicheva[62], P. Karczmarczyk[34], E. Karpechev[62],
U. Kebschull[73], R. Keidel[46], M. Keil[34], B. Ketzer[42], Z. Khabanova[88], A.M. Khan[6], S. Khan[17],
S.A. Khan[141], A. Khanzadeev[96], Y. Kharlov[89], A. Khatun[17], A. Khuntia[49,118], B. Kileng[36],
B. Kim[60], B. Kim[133], D. Kim[147], D.J. Kim[126], E.J. Kim[13], H. Kim[147], J. Kim[147], J.S. Kim[40],
J. Kim[102], J. Kim[147], J. Kim[13], M. Kim[102], S. Kim[19], T. Kim[147], T. Kim[147], S. Kirsch[39],
I. Kisel[39], S. Kiselev[90], A. Kisiel[142], J.L. Klay[5], C. Klein[68], J. Klein[58], S. Klein[78],
C. Klein-Bösing[144], S. Klewin[102], A. Kluge[34], M.L. Knichel[34], A.G. Knospe[125], C. Kobdaj[115],
M.K. Köhler[102], T. Kollegger[105], A. Kondratyev[74], N. Kondratyeva[91], E. Kondratyuk[89],
P.J. Konopka[34], L. Koska[116], O. Kovalenko[83], V. Kovalenko[112], M. Kowalski[118], I. Králik[64],
A. Kravčáková[38], L. Kreis[105], M. Krivda[64,109], F. Krizek[93], K. Krizkova Gajdosova[37],
M. Krüger[68], E. Kryshen[96], M. Krzewicki[39], A.M. Kubera[95], V. Kučera[60], C. Kuhn[136],
P.G. Kuijer[88], L. Kumar[98], S. Kumar[48], S. Kundu[84], P. Kurashvili[83], A. Kurepin[62],
A.B. Kurepin[62], S. Kushpil[93], J. Kvapil[109], M.J. Kweon[60], J.Y. Kwon[60], Y. Kwon[147], S.L. La
Pointe[39], P. La Rocca[28], Y.S. Lai[78], R. Langoy[129], K. Lapidus[34,146], A. Lardeux[21], P. Larionov[51],
E. Laudi[34], R. Lavicka[37], T. Lazareva[112], R. Lea[25], L. Leardini[102], S. Lee[147], F. Lehas[88],
S. Lehner[113], J. Lehrbach[39], R.C. Lemmon[92], I. León Monzón[120], E.D. Lesser[20], M. Lettrich[34],
P. Lévai[145], X. Li[12], X.L. Li[6], J. Lien[129], R. Lietava[109], B. Lim[18], S. Lindal[21], V. Lindenstruth[39],
S.W. Lindsay[127], C. Lippmann[105], M.A. Lisa[95], V. Litichevskyi[43], A. Liu[78], S. Liu[95],
W.J. Llope[143], I.M. Lofnes[22], V. Loginov[91], C. Loizides[94], P. Loncar[35], X. Lopez[134], E. López
Torres[8], P. Luettig[68], J.R. Luhder[144], M. Lunardon[29], G. Luparello[59], M. Lupi[73], A. Maevskaya[62],
M. Mager[34], S.M. Mahmood[21], T. Mahmoud[42], A. Maire[136], R.D. Majka[146], M. Malaev[96],
Q.W. Malik[21], L. Malinina[74, iii], D. Mal'Kevich[90], P. Malzacher[105], A. Mamonov[107],
G. Mandaglio[55], V. Manko[86], F. Manso[134], V. Manzari[52], Y. Mao[6], M. Marchisone[135], J. Mareš[66],
G.V. Margagliotti[25], A. Margotti[53], J. Margutti[63], A. Marín[105], C. Markert[119], M. Marquard[68],
N.A. Martin[102], P. Martinengo[34], J.L. Martinez[125], M.I. Martínez[44], G. Martínez García[114],

M. Martinez Pedreira[34], S. Masciocchi[105], M. Masera[26], A. Masoni[54], L. Massacrier[61], E. Masson[114], A. Mastroserio[138], A.M. Mathis[103,117], O. Matonoha[79], P.F.T. Matuoka[121], A. Matyja[118], C. Mayer[118], M. Mazzilli[33], M.A. Mazzoni[57], A.F. Mechler[68], F. Meddi[23], Y. Melikyan[91], A. Menchaca-Rocha[71], E. Meninno[30], M. Meres[14], S. Mhlanga[124], Y. Miake[133], L. Micheletti[26], M.M. Mieskolainen[43], D.L. Mihaylov[103], K. Mikhaylov[74,90], A. Mischke[63, i], A.N. Mishra[69], D. Miśkowiec[105], C.M. Mitu[67], A. Modak[3], N. Mohammadi[34], A.P. Mohanty[63], B. Mohanty[84], M. Mohisin Khan[17, iv], M. Mondal[141], M.M. Mondal[65], C. Mordasini[103], D.A. Moreira De Godoy[144], L.A.P. Moreno[44], S. Moretto[29], A. Morreale[114], A. Morsch[34], T. Mrnjavac[34], V. Muccifora[51], E. Mudnic[35], D. Mühlheim[144], S. Muhuri[141], J.D. Mulligan[78,146], M.G. Munhoz[121], K. Münning[42], R.H. Munzer[68], H. Murakami[132], S. Murray[72], L. Musa[34], J. Musinsky[64], C.J. Myers[125], J.W. Myrcha[142], B. Naik[48], R. Nair[83], B.K. Nandi[48], R. Nania[10,53], E. Nappi[52], M.U. Naru[15], A.F. Nassirpour[79], H. Natal da Luz[121], C. Nattrass[130], R. Nayak[48], T.K. Nayak[84,141], S. Nazarenko[107], R.A. Negrao De Oliveira[68], L. Nellen[69], S.V. Nesbo[36], G. Neskovic[39], B.S. Nielsen[87], S. Nikolaev[86], S. Nikulin[86], V. Nikulin[96], F. Noferini[10,53], P. Nomokonov[74], G. Nooren[63], J. Norman[77], P. Nowakowski[142], A. Nyanin[86], J. Nystrand[22], M. Ogino[80], A. Ohlson[102], J. Oleniacz[142], A.C. Oliveira Da Silva[121], M.H. Oliver[146], C. Oppedisano[58], R. Orava[43], A. Ortiz Velasquez[69], A. Oskarsson[79], J. Otwinowski[118], K. Oyama[80], Y. Pachmayer[102], V. Pacik[87], D. Pagano[140], G. Paić[69], P. Palni[6], J. Pan[143], A.K. Pandey[48], S. Panebianco[137], V. Papikyan[1], P. Pareek[49], J. Park[60], J.E. Parkkila[126], S. Parmar[98], A. Passfeld[144], S.P. Pathak[125], R.N. Patra[141], B. Paul[24,58], H. Pei[6], T. Peitzmann[63], X. Peng[6], L.G. Pereira[70], H. Pereira Da Costa[137], D. Peresunko[86], G.M. Perez[8], E. Perez Lezama[68], V. Peskov[68], Y. Pestov[4], V. Petráček[37], M. Petrovici[47], R.P. Pezzi[70], S. Piano[59], M. Pikna[14], P. Pillot[114], L.O.D.L. Pimentel[87], O. Pinazza[34,53], L. Pinsky[125], C. Pinto[28], S. Pisano[51], D.B. Piyarathna[125], M. Płoskoń[78], M. Planinic[97], F. Pliquett[68], J. Pluta[142], S. Pochybova[145], M.G. Poghosyan[94], B. Polichtchouk[89], N. Poljak[97], W. Poonsawat[115], A. Pop[47], H. Poppenborg[144], S. Porteboeuf-Houssais[134], V. Pozdniakov[74], S.K. Prasad[3], R. Preghenella[53], F. Prino[58], C.A. Pruneau[143], I. Pshenichnov[62], M. Puccio[26,34], V. Punin[107], K. Puranapanda[141], J. Putschke[143], R.E. Quishpe[125], S. Ragoni[109], S. Raha[3], S. Rajput[99], J. Rak[126], A. Rakotozafindrabe[137], L. Ramello[32], F. Rami[136], R. Raniwala[100], S. Raniwala[100], S.S. Räsänen[43], B.T. Rascanu[68], R. Rath[49], V. Ratza[42], I. Ravasenga[31], K.F. Read[94,130], K. Redlich[83, v], A. Rehman[22], P. Reichelt[68], F. Reidt[34], X. Ren[6], R. Renfordt[68], A. Reshetin[62], J.-P. Revol[10], K. Reygers[102], V. Riabov[96], T. Richert[79,87], M. Richter[21], P. Riedler[34], W. Riegler[34], F. Riggi[28], C. Ristea[67], S.P. Rode[49], M. Rodríguez Cahuantzi[44], K. Røed[21], R. Rogalev[89], E. Rogochaya[74], D. Rohr[34], D. Röhrich[22], P.S. Rokita[142], F. Ronchetti[51], E.D. Rosas[69], K. Roslon[142], P. Rosnet[134], A. Rossi[29], A. Rotondi[139], F. Roukoutakis[82], A. Roy[49], P. Roy[108], O.V. Rueda[79], R. Rui[25], B. Rumyantsev[74], A. Rustamov[85], E. Ryabinkin[86], Y. Ryabov[96], A. Rybicki[118], H. Rytkonen[126], S. Sadhu[141], S. Sadovsky[89], K. Šafařík[34,37], S.K. Saha[141], B. Sahoo[48], P. Sahoo[48,49], R. Sahoo[49], S. Sahoo[65], P.K. Sahu[65], J. Saini[141], S. Sakai[133], S. Sambyal[99], V. Samsonov[91,96], A. Sandoval[71], A. Sarkar[72], D. Sarkar[143], N. Sarkar[141], P. Sarma[41], V.M. Sarti[103], M.H.P. Sas[63], E. Scapparone[53], B. Schaefer[94], J. Schambach[119], H.S. Scheid[68], C. Schiaua[47], R. Schicker[102], A. Schmah[102], C. Schmidt[105], H.R. Schmidt[101], M.O. Schmidt[102], M. Schmidt[101], N.V. Schmidt[68,94], A.R. Schmier[130], J. Schukraft[34,87], Y. Schutz[34,136], K. Schwarz[105], K. Schweda[105], G. Scioli[27], E. Scomparin[58], M. Šefčík[38], J.E. Seger[16], Y. Sekiguchi[132], D. Sekihata[45,132], I. Selyuzhenkov[91,105], S. Senyukov[136], D. Serebryakov[62], E. Serradilla[71], P. Sett[48], A. Sevcenco[67], A. Shabanov[62], A. Shabetai[114], R. Shahoyan[34], W. Shaikh[108], A. Shangaraev[89], A. Sharma[98], A. Sharma[99], H. Sharma[118], M. Sharma[99], N. Sharma[98], A.I. Sheikh[141], K. Shigaki[45], M. Shimomura[81], S. Shirinkin[90], Q. Shou[111], Y. Sibiriak[86], S. Siddhanta[54], T. Siemiarczuk[83], D. Silvermyr[79],

C. Silvestre[77], G. Simatovic[88], G. Simonetti[34,103], R. Singh[84], R. Singh[99], V.K. Singh[141],
V. Singhal[141], T. Sinha[108], B. Sitar[14], M. Sitta[32], T.B. Skaali[21], M. Slupecki[126], N. Smirnov[146],
R.J.M. Snellings[63], T.W. Snellman[126], J. Sochan[116], C. Soncco[110], J. Song[60,125],
A. Songmoolnak[115], F. Soramel[29], S. Sorensen[130], I. Sputowska[118], J. Stachel[102], I. Stan[67],
P. Stankus[94], P.J. Steffanic[130], E. Stenlund[79], D. Stocco[114], M.M. Storetvedt[36], P. Strmen[14],
A.A.P. Suaide[121], T. Sugitate[45], C. Suire[61], M. Suleymanov[15], M. Suljic[34], R. Sultanov[90],
M. Šumbera[93], S. Sumowidagdo[50], K. Suzuki[113], S. Swain[65], A. Szabo[14], I. Szarka[14],
U. Tabassam[15], G. Taillepied[134], J. Takahashi[122], G.J. Tambave[22], S. Tang[6,134], M. Tarhini[114],
M.G. Tarzila[47], A. Tauro[34], G. Tejeda Muñoz[44], A. Telesca[34], C. Terrevoli[29,125], D. Thakur[49],
S. Thakur[141], D. Thomas[119], F. Thoresen[87], R. Tieulent[135], A. Tikhonov[62], A.R. Timmins[125],
A. Toia[68], N. Topilskaya[62], M. Toppi[51], F. Torales-Acosta[20], S.R. Torres[120], A. Trifiro[55],
S. Tripathy[49], T. Tripathy[48], S. Trogolo[26,29], G. Trombetta[33], L. Tropp[38], V. Trubnikov[2],
W.H. Trzaska[126], T.P. Trzcinski[142], B.A. Trzeciak[63], T. Tsuji[132], A. Tumkin[107], R. Turrisi[56],
T.S. Tveter[21], K. Ullaland[22], E.N. Umaka[125], A. Uras[135], G.L. Usai[24], A. Utrobicic[97],
M. Vala[38,116], N. Valle[139], S. Vallero[58], N. van der Kolk[63], L.V.R. van Doremalen[63], M. van
Leeuwen[63], P. Vande Vyvre[34], D. Varga[145], Z. Varga[145], M. Varga-Kofarago[145], A. Vargas[44],
M. Vargyas[126], R. Varma[48], M. Vasileiou[82], A. Vasiliev[86], O. Vázquez Doce[103,117],
V. Vechernin[112], A.M. Veen[63], E. Vercellin[26], S. Vergara Limón[44], L. Vermunt[63], R. Vernet[7],
R. Vértesi[145], M.G.D.L.C. Vicencio[9], L. Vickovic[35], J. Viinikainen[126], Z. Vilakazi[131], O. Villalobos
Baillie[109], A. Villatoro Tello[44], G. Vino[52], A. Vinogradov[86], T. Virgili[30], V. Vislavicius[87],
A. Vodopyanov[74], B. Volkel[34], M.A. Völkl[101], K. Voloshin[90], S.A. Voloshin[143], G. Volpe[33], B. von
Haller[34], I. Vorobyev[103], D. Voscek[116], J. Vrláková[38], B. Wagner[22], Y. Watanabe[133], M. Weber[113],
S.G. Weber[105,144], A. Wegrzynek[34], D.F. Weiser[102], S.C. Wenzel[34], J.P. Wessels[144],
E. Widmann[113], J. Wiechula[68], J. Wikne[21], G. Wilk[83], J. Wilkinson[53], G.A. Willems[34],
E. Willsher[109], B. Windelband[102], W.E. Witt[130], Y. Wu[128], R. Xu[6], S. Yalcin[76], K. Yamakawa[45],
S. Yang[22], S. Yano[137], Z. Yin[6], H. Yokoyama[63,133], I.-K. Yoo[18], J.H. Yoon[60], S. Yuan[22],
A. Yuncu[102], V. Yurchenko[2], V. Zaccolo[25,58], A. Zaman[15], C. Zampolli[34], H.J.C. Zanoli[63,121],
N. Zardoshti[34], A. Zarochentsev[112], P. Závada[66], N. Zaviyalov[107], H. Zbroszczyk[142], M. Zhalov[96],
X. Zhang[6], Z. Zhang[6], C. Zhao[21], V. Zherebchevskii[112], N. Zhigareva[90], D. Zhou[6], Y. Zhou[87],
Z. Zhou[22], J. Zhu[6], Y. Zhu[6], A. Zichichi[10,27], M.B. Zimmermann[34], G. Zinovjev[2], N. Zurlo[140],

[i]   Deceased
[ii] Dipartimento DET del Politecnico di Torino, Turin, Italy
[iii] M.V. Lomonosov Moscow State University, D.V. Skobeltsyn Institute of Nuclear, Physics, Moscow,
      Russia
[iv] Department of Applied Physics, Aligarh Muslim University, Aligarh, India
[v]   Institute of Theoretical Physics, University of Wroclaw, Poland

1   A.I. Alikhanyan National Science Laboratory (Yerevan Physics Institute) Foundation, Yerevan,
    Armenia
2   Bogolyubov Institute for Theoretical Physics, National Academy of Sciences of Ukraine, Kiev,
    Ukraine
3   Bose Institute, Department of Physics and Centre for Astroparticle Physics and Space Science
    (CAPSS), Kolkata, India
4   Budker Institute for Nuclear Physics, Novosibirsk, Russia
5   California Polytechnic State University, San Luis Obispo, California, United States
6   Central China Normal University, Wuhan, China
7   Centre de Calcul de l'IN2P3, Villeurbanne, Lyon, France
8   Centro de Aplicaciones Tecnológicas y Desarrollo Nuclear (CEADEN), Havana, Cuba

JHEP12(2019)092

9 *Centro de Investigación y de Estudios Avanzados (CINVESTAV), Mexico City and Mérida, Mexico*

10 *Centro Fermi — Museo Storico della Fisica e Centro Studi e Ricerche "Enrico Fermi', Rome, Italy*

11 *Chicago State University, Chicago, Illinois, United States*

12 *China Institute of Atomic Energy, Beijing, China*

13 *Chonbuk National University, Jeonju, Republic of Korea*

14 *Comenius University Bratislava, Faculty of Mathematics, Physics and Informatics, Bratislava, Slovakia*

15 *COMSATS University Islamabad, Islamabad, Pakistan*

16 *Creighton University, Omaha, Nebraska, United States*

17 *Department of Physics, Aligarh Muslim University, Aligarh, India*

18 *Department of Physics, Pusan National University, Pusan, Republic of Korea*

19 *Department of Physics, Sejong University, Seoul, Republic of Korea*

20 *Department of Physics, University of California, Berkeley, California, United States*

21 *Department of Physics, University of Oslo, Oslo, Norway*

22 *Department of Physics and Technology, University of Bergen, Bergen, Norway*

23 *Dipartimento di Fisica dell'Università 'La Sapienza' and Sezione INFN, Rome, Italy*

24 *Dipartimento di Fisica dell'Università and Sezione INFN, Cagliari, Italy*

25 *Dipartimento di Fisica dell'Università and Sezione INFN, Trieste, Italy*

26 *Dipartimento di Fisica dell'Università and Sezione INFN, Turin, Italy*

27 *Dipartimento di Fisica e Astronomia dell'Università and Sezione INFN, Bologna, Italy*

28 *Dipartimento di Fisica e Astronomia dell'Università and Sezione INFN, Catania, Italy*

29 *Dipartimento di Fisica e Astronomia dell'Università and Sezione INFN, Padova, Italy*

30 *Dipartimento di Fisica 'E.R. Caianiello' dell'Università and Gruppo Collegato INFN, Salerno, Italy*

31 *Dipartimento DISAT del Politecnico and Sezione INFN, Turin, Italy*

32 *Dipartimento di Scienze e Innovazione Tecnologica dell'Università del Piemonte Orientale and INFN Sezione di Torino, Alessandria, Italy*

33 *Dipartimento Interateneo di Fisica 'M. Merlin' and Sezione INFN, Bari, Italy*

34 *European Organization for Nuclear Research (CERN), Geneva, Switzerland*

35 *Faculty of Electrical Engineering, Mechanical Engineering and Naval Architecture, University of Split, Split, Croatia*

36 *Faculty of Engineering and Science, Western Norway University of Applied Sciences, Bergen, Norway*

37 *Faculty of Nuclear Sciences and Physical Engineering, Czech Technical University in Prague, Prague, Czech Republic*

38 *Faculty of Science, P.J. Šafárik University, Košice, Slovakia*

39 *Frankfurt Institute for Advanced Studies, Johann Wolfgang Goethe-Universität Frankfurt, Frankfurt, Germany*

40 *Gangneung-Wonju National University, Gangneung, Republic of Korea*

41 *Gauhati University, Department of Physics, Guwahati, India*

42 *Helmholtz-Institut für Strahlen- und Kernphysik, Rheinische Friedrich-Wilhelms-Universität Bonn, Bonn, Germany*

43 *Helsinki Institute of Physics (HIP), Helsinki, Finland*

44 *High Energy Physics Group, Universidad Autónoma de Puebla, Puebla, Mexico*

45 *Hiroshima University, Hiroshima, Japan*

46 *Hochschule Worms, Zentrum für Technologietransfer und Telekommunikation (ZTT), Worms, Germany*

47 *Horia Hulubei National Institute of Physics and Nuclear Engineering, Bucharest, Romania*

48 *Indian Institute of Technology Bombay (IIT), Mumbai, India*

49 *Indian Institute of Technology Indore, Indore, India*

50 *Indonesian Institute of Sciences, Jakarta, Indonesia*

51 *INFN, Laboratori Nazionali di Frascati, Frascati, Italy*

52 *INFN, Sezione di Bari, Bari, Italy*

53 INFN, Sezione di Bologna, Bologna, Italy

54 INFN, Sezione di Cagliari, Cagliari, Italy

55 INFN, Sezione di Catania, Catania, Italy

56 INFN, Sezione di Padova, Padova, Italy

57 INFN, Sezione di Roma, Rome, Italy

58 INFN, Sezione di Torino, Turin, Italy

59 INFN, Sezione di Trieste, Trieste, Italy

60 Inha University, Incheon, Republic of Korea

61 Institut de Physique Nucléaire d'Orsay (IPNO), Institut National de Physique Nucléaire et de
    Physique des Particules (IN2P3/CNRS), Université de Paris-Sud, Université Paris-Saclay, Orsay,
    France

62 Institute for Nuclear Research, Academy of Sciences, Moscow, Russia

63 Institute for Subatomic Physics, Utrecht University/Nikhef, Utrecht, Netherlands

64 Institute of Experimental Physics, Slovak Academy of Sciences, Košice, Slovakia

65 Institute of Physics, Homi Bhabha National Institute, Bhubaneswar, India

66 Institute of Physics of the Czech Academy of Sciences, Prague, Czech Republic

67 Institute of Space Science (ISS), Bucharest, Romania

68 Institut für Kernphysik, Johann Wolfgang Goethe-Universität Frankfurt, Frankfurt, Germany

69 Instituto de Ciencias Nucleares, Universidad Nacional Autónoma de México, Mexico City, Mexico

70 Instituto de Física, Universidade Federal do Rio Grande do Sul (UFRGS), Porto Alegre, Brazil

71 Instituto de Física, Universidad Nacional Autónoma de México, Mexico City, Mexico

72 iThemba LABS, National Research Foundation, Somerset West, South Africa

73 Johann-Wolfgang-Goethe Universität Frankfurt Institut für Informatik, Fachbereich Informatik und
    Mathematik, Frankfurt, Germany

74 Joint Institute for Nuclear Research (JINR), Dubna, Russia

75 Korea Institute of Science and Technology Information, Daejeon, Republic of Korea

76 KTO Karatay University, Konya, Turkey

77 Laboratoire de Physique Subatomique et de Cosmologie, Université Grenoble-Alpes, CNRS-IN2P3,
    Grenoble, France

78 Lawrence Berkeley National Laboratory, Berkeley, California, United States

79 Lund University Department of Physics, Division of Particle Physics, Lund, Sweden

80 Nagasaki Institute of Applied Science, Nagasaki, Japan

81 Nara Women's University (NWU), Nara, Japan

82 National and Kapodistrian University of Athens, School of Science, Department of Physics, Athens,
    Greece

83 National Centre for Nuclear Research, Warsaw, Poland

84 National Institute of Science Education and Research, Homi Bhabha National Institute, Jatni, India

85 National Nuclear Research Center, Baku, Azerbaijan

86 National Research Centre Kurchatov Institute, Moscow, Russia

87 Niels Bohr Institute, University of Copenhagen, Copenhagen, Denmark

88 Nikhef, National institute for subatomic physics, Amsterdam, Netherlands

89 NRC Kurchatov Institute IHEP, Protvino, Russia

90 NRC "Kurchatov Institute" — ITEP, Moscow, Russia

91 NRNU Moscow Engineering Physics Institute, Moscow, Russia

92 Nuclear Physics Group, STFC Daresbury Laboratory, Daresbury, United Kingdom

93 Nuclear Physics Institute of the Czech Academy of Sciences, Řež u Prahy, Czech Republic

94 Oak Ridge National Laboratory, Oak Ridge, Tennessee, United States

95 Ohio State University, Columbus, Ohio, United States

96 Petersburg Nuclear Physics Institute, Gatchina, Russia

97 Physics department, Faculty of science, University of Zagreb, Zagreb, Croatia

98 Physics Department, Panjab University, Chandigarh, India

99 Physics Department, University of Jammu, Jammu, India

[100] *Physics Department, University of Rajasthan, Jaipur, India*
[101] *Physikalisches Institut, Eberhard-Karls-Universität Tübingen, Tübingen, Germany*
[102] *Physikalisches Institut, Ruprecht-Karls-Universität Heidelberg, Heidelberg, Germany*
[103] *Physik Department, Technische Universität München, Munich, Germany*
[104] *Politecnico di Bari, Bari, Italy*
[105] *Research Division and ExtreMe Matter Institute EMMI, GSI Helmholtzzentrum für Schwerionenforschung GmbH, Darmstadt, Germany*
[106] *Rudjer Bošković Institute, Zagreb, Croatia*
[107] *Russian Federal Nuclear Center (VNIIEF), Sarov, Russia*
[108] *Saha Institute of Nuclear Physics, Homi Bhabha National Institute, Kolkata, India*
[109] *School of Physics and Astronomy, University of Birmingham, Birmingham, United Kingdom*
[110] *Sección Física, Departamento de Ciencias, Pontificia Universidad Católica del Perú, Lima, Peru*
[111] *Shanghai Institute of Applied Physics, Shanghai, China*
[112] *St. Petersburg State University, St. Petersburg, Russia*
[113] *Stefan Meyer Institut für Subatomare Physik (SMI), Vienna, Austria*
[114] *SUBATECH, IMT Atlantique, Université de Nantes, CNRS-IN2P3, Nantes, France*
[115] *Suranaree University of Technology, Nakhon Ratchasima, Thailand*
[116] *Technical University of Košice, Košice, Slovakia*
[117] *Technische Universität München, Excellence Cluster 'Universe', Munich, Germany*
[118] *The Henryk Niewodniczanski Institute of Nuclear Physics, Polish Academy of Sciences, Cracow, Poland*
[119] *The University of Texas at Austin, Austin, Texas, United States*
[120] *Universidad Autónoma de Sinaloa, Culiacán, Mexico*
[121] *Universidade de São Paulo (USP), São Paulo, Brazil*
[122] *Universidade Estadual de Campinas (UNICAMP), Campinas, Brazil*
[123] *Universidade Federal do ABC, Santo Andre, Brazil*
[124] *University of Cape Town, Cape Town, South Africa*
[125] *University of Houston, Houston, Texas, United States*
[126] *University of Jyväskylä, Jyväskylä, Finland*
[127] *University of Liverpool, Liverpool, United Kingdom*
[128] *University of Science and Techonology of China, Hefei, China*
[129] *University of South-Eastern Norway, Tonsberg, Norway*
[130] *University of Tennessee, Knoxville, Tennessee, United States*
[131] *University of the Witwatersrand, Johannesburg, South Africa*
[132] *University of Tokyo, Tokyo, Japan*
[133] *University of Tsukuba, Tsukuba, Japan*
[134] *Université Clermont Auvergne, CNRS/IN2P3, LPC, Clermont-Ferrand, France*
[135] *Université de Lyon, Université Lyon 1, CNRS/IN2P3, IPN-Lyon, Villeurbanne, Lyon, France*
[136] *Université de Strasbourg, CNRS, IPHC UMR 7178, F-67000 Strasbourg, France, Strasbourg, France*
[137] *Université Paris-Saclay Centre d'Etudes de Saclay (CEA), IRFU, Départment de Physique Nucléaire (DPhN), Saclay, France*
[138] *Università degli Studi di Foggia, Foggia, Italy*
[139] *Università degli Studi di Pavia, Pavia, Italy*
[140] *Università di Brescia, Brescia, Italy*
[141] *Variable Energy Cyclotron Centre, Homi Bhabha National Institute, Kolkata, India*
[142] *Warsaw University of Technology, Warsaw, Poland*
[143] *Wayne State University, Detroit, Michigan, United States*
[144] *Westfälische Wilhelms-Universität Münster, Institut für Kernphysik, Münster, Germany*
[145] *Wigner Research Centre for Physics, Hungarian Academy of Sciences, Budapest, Hungary*
[146] *Yale University, New Haven, Connecticut, United States*
[147] *Yonsei University, Seoul, Republic of Korea*